Validated prediction of weld residual stresses in austenitic steel pipe girth welds before and after thermal ageing, part 1: Mock-up manufacture, residual stress measurements, and materials characterisation

Journal Item

Validated prediction of weld residual stresses in austenitic steel pipe girth welds before and after thermal ageing, Part 1: mock-up manufacture, residual stress measurements, and materials characterisation

M C Smith[a], O Muransky[b,c], Q Xiong[a], J Mathew[d], C Austin[e]

a) The University of Manchester

b) Australian Science and Technology Organization (ANSTO), Sydney, NSW, Australia

c) School of Materials Science and Engineering, UNSW Sydney, Sydney, Australia

d) Faculty of Engineering and Computing, Coventry University, Priory Street, Coventry CV1 5FB, UK

e) Wood Group, plc

1 Abstract

A series of engineering-scale multi-pass pipe girth weld mock-ups were manufactured using conventional manual metal arc techniques from Esshete 1250 austenitic steel. They were characterised in detail, in order to provide validation benchmarks for finite element prediction of weld residual stresses. The fabrication sequence comprised initial solution heat treatment and quenching, manufacture of five closely spaced girth welds in a single assembly, and then separation into five individual weldments. Detailed welding records were kept, to allow subsequent calibration of weld heat source models. Residual stresses were measured using diverse methods (incremental deep hole drilling and the contour method), in both the as-welded condition and after thermal ageing at 650°C. The measurements showed good agreement, providing reliable validation targets for predicted residual stresses in both states. Detailed mechanical property characterisation was performed on both parent material and weld metal, comprising monotonic and isothermal cyclic testing over a range of temperatures from ambient up to 1000°C. The test data were used to derive a range of Lemaitre-Chaboche mixed isotropic-kinematic model parameter sets for use in finite element simulation. These welds and their supporting characterisation comprise a reliable benchmark for weld residual stress simulation in an engineering-scale weldment.

2 Introduction

Finite element methods are used increasingly to predict weld residual stresses for use in weld structural performance assessments [1, 2], since they offer the prospect of more accurate, less

conservative residual stress profiles than the upper bounds currently provided in structural integrity assessment procedures such as R6 [3] and API 579 [4]. However, uncertainties in finite element predictions remain a serious concern. The R6 procedure includes guidelines for finite element prediction of weld residual stresses [5, 6] and imposes strict validation requirements on such numerical predictions. The level of validation required depends on the structural integrity significance of weld residual stresses in the weldment being considered, but wholly unvalidated finite element predictions may not be used in structural integrity assessments of safety-critical components.

Validation of finite element weld residual stress predictions requires representative, closely characterized mock-ups with reliable and repeatable residual stress measurements, preferably made using diverse methods with different characteristic errors (for example, diffraction-based and strain relief methods). The NeT collaboration has produced several high quality benchmarks with large bodies of residual stress measurements [7-14]. These include:

- NeT TG1: a single finite length gas tungsten arc (GTAW) weld bead made with AISI 316L welding wire, laid on an AISI 316L austenitic steel plate
- Net TG4: a three-pass GTAW weld made with AISI 316L welding wire, laid in a finite length slot in an AISI 316L(N) austenitic steel plate
- NeT TG5: a beam specimen in SA508 Gr 3 Cl 1 low alloy pressure vessel steel with a single autogenous GTAW weld pass along one edge
- NeT TG6: a three-pass GTAW weld made with Alloy 82 welding wire, laid in a finite length slot in an alloy 600 nickel alloy plate

NeT adopt the approach of characterizing their benchmarks to a very high level. Multiple residual stress measurements using diverse techniques are accompanied by detailed characterization of the welding process and its associated thermal transients, and extensive materials property testing. This approach ensures both that finite element simulations made to predict the weld residual stresses have the minimum possible uncertainty in their input data, and that the validation data for the simulation end products, residual stresses and distortions, are accurate and representative.

The NeT benchmarks are all small weldments with limited numbers of weld passes, so cannot act as fully representative validation examples for multi-pass welds in large engineering structures. These require larger scale mock-ups. Such components tend to be rare, because of the costs involved in their manufacture, the difficulties encountered in making reliable, diverse and repeatable residual stress measurements in large components, and the burden of detailed material property characterization required for reliable benchmarking of simulations. Recent examples are the programmes run independently by British Energy (now EDF

Energy) in the UK [15-19] and by EPRI/NRC in the USA [20, 21], both examining residual stresses in PWR primary circuit dissimilar metal welds. These programmes delivered mixed results: while it is possible to obtain accurate predicted residual stresses [18], considerable scatter in predicted stresses can occur [20, 21], and it can be extremely difficult in these complex weldments to identify and account for all the sources of analysis variation.

Plain girth welds in austenitic steels are usually considered to be a more tractable problem. Indeed, Bouchard [22] has developed an analytical formulation for through-thickness residual stress profiles in conventional austenitic stainless steel pipe butt welds, intended to be used for defect tolerance assessment. This formulation is based on a combination of mock-up residual stress measurements on large-scale mock-ups, and finite element simulation, using data available up to approximately 2001 (for example, see [23]). Although the supporting residual stress measurements were made on nine separate weldments, they were limited to techniques available at the time, and in some cases diverse measurements were either not feasible, or they produced divergent results. The simulations underlying [22] also, of course, used techniques and knowledge available at the time.

The residual stress measurement techniques available for thick section welds have improved significantly in recent years. The conventional deep hole drilling technique, which was applied to the majority of mock-ups considered by Bouchard, is susceptible to plasticity induced errors when the residual stresses approach yield, and the incremental deep hole drilling method has been developed to minimize such errors [24]. Similarly, the contour method [25] has undergone continuous development, and can now be applied to large-scale structures such as dissimilar metal welded nozzles and pipe butt welds.

A number of thick-walled austenitic steel pipe girth weld mock-ups have been manufactured by British Energy (now EDF Energy) for an internal research programme, and then utilized by the STYLE Framework 7 project [26]. They include both five short pipes with plain circumferential butt welds and five longer pipes with circumferential butt welds containing weld repairs. The mock-ups were fabricated under carefully controlled conditions, and residual stress measurements made using diverse techniques in both the as-welded state, and after thermal ageing at high temperature to simulate the service conditions. In-service creep relaxation of residual stresses is an important phenomenon because the steel used to fabricate the mock-ups, Esshete 1250, is potentially susceptible to creep or reheat cracking in the weld metal and adjacent HAZ, driven by residual stress relaxation.

An extensive programme of mechanical property evaluation was performed in parallel with mock-up manufacture and characterisation, on both parent material and the matching manual metal arc (MMA) weld metal [27].

These mock-ups offer an opportunity to assess the state of the art in weld residual stress prediction in a geometry that is more relevant to plant components than the small scale benchmark specimens studied under the auspices of NeT. This assessment can cover both start-of-life residual stresses and the prediction of creep relaxation during high-temperature service.

This study is reported in two parts:

1. Part 1 (this paper) describes the manufacture, characterisation, and residual stress measurements performed on the pipe girth weld mock-ups, reports the detailed mechanical testing performed to establish the cyclic hardening behaviour of both parent material and MMA weld metal, and describes the approaches used to fit the parameters for mixed isotropic-kinematic hardening models.
2. Part 2 describes the simulation campaign. This was performed in two stages. Stage 1 investigated the impact of the complex manufacturing history on the predicted residual stress state, while Stage 2 examined the impact of the material hardening model and creep deformation behaviour on the residual stress states after completion of manufacture, and after long term high temperature exposure.

The study is based primarily on the plain circumferential butt welds in the short pipes, and these are described in full. The circumferential butt welds in the long pipe specimens were identical to those in the short pipes. Residual stresses were also measured in the long pipes after high temperature exposure, and measurements made in the circumferential butt welds remote from weld repairs are also discussed here.

3 Description of mock-ups

3.1 Short pipes containing plain circumferential butt welds

First, a welded pipe assembly was fabricated from Esshete 1250, an austenitic stainless steel with added vanadium and niobium to increase its high-temperature strength. The layout of the completed welded pipe assembly, consisting of 4 full-length (200 mm long) and 2 half-length (100 mm long) pipes and five welds, is shown in Figure 1. The outer diameter was 180 mm and wall thickness 35 mm, giving $R_m/t=2.1$. After completion of welding the assembly was cut into five individual mock-ups, each of length 200 mm, see Figure 2.

The manufacturing process comprised the following steps:

1) Rough machining. The material was supplied as ϕ185 mm bar stock, so the bar was first cut to length and then bore-machined to 105 mm inside diameter (4x 200 mm length and 2x 100 mm length).

2) Quenching. The rough-machined cylinders were solution heat treated at 1080°C in air for 30 min followed by water quenching. The heating rate for the solution treatment was 50°C/h. A number of the specimens were instrumented to record the quenching temperature transients. Thermocouples were peened into holes on the cylinder surfaces, one on an end-face at mid-radius, and one on the outer bore at mid-length. Typical measured responses are shown in Figure 3.

3) Final Machining. After heat treatment, the cylinders were machined to their final dimensions, removing equal amounts of material from inner and outer surfaces to achieve an outer diameter of 180 mm and a wall thickness of 35 mm. Conventional J-groove weld preparations with a 15° sidewall angle were machined at each end of the long sections and at one end of the short sections, see Figure 4a.

4) Welding. The machined cylinders were mounted on a rotating manipulator (see Figure 1), and the welds were completed in the sequence shown, starting with weld 1 on the right-hand side and finishing with weld 5 in the middle of the entire assembly. Welds were made in the 1G (vertical) position with the pipe rotated. The root and first fill passes were deposited via a manual TIG process using 2.4 mm diameter Esshete 1250 filler rods. Subsequent weld fill and capping passes were deposited using an MMA process with 3.25 mm, 4.0 mm, and 5.0 mm diameter ESAB OK 69.86 electrodes. All the welding passes were deposited in the same direction. The welding parameters for all weld passes were recorded. The inter-pass temperature was measured using a contact thermometer on the weld surface at the start position, prior to the deposition of the subsequent welding pass. All welds were made using the same procedure and bead lay-up, with the exception of the capping beads. As can be seen from Figure 1, three welds were made with two capping passes, and two were made with three lower heat input passes. Representative measured welding parameters are given in the Appendix.

5) Grinding. Upon completion of welding, the root bead reinforcement was ground flush (i.e. the root pass protrusion was removed). The weld caps were left intact.

6) Cutting. The completed pipe assembly was then cut into five equal-length test specimens, each having a girth weld at mid-length.

7) Non-destructive examination. Both liquid penetrant and X-ray radiography were used. No significant defects were observed except in pipe CY5/CY9 where the radiography showed linear indications at several locations at the root.

8) Ageing: Three of the test specimens were thermally aged at 650°C for at least 10,000 hours.

The manufacturing records included a detailed photographic record, thermocouple measurements during the quenching process, measured welding parameters, measured inter-pass temperatures, and weld bead lay-up maps for individual welds. A weld transverse macrograph was prepared from pipe CY7/CY6, see Figure 4. Because no thermocouple arrays were attached to the specimens during welding, no transient temperature data were available for calibration of finite element heat source models. This is a departure from best practice as established by NeT [11, 28], but is a common situation for large scale weldments.

3.2 Long pipes containing weld repairs

Manufacture of these mock-ups followed a similar procedure to the short pipes, except a finite length weld repair was made to the circumferential butt weld prior to residual stress measurements in the as-welded condition and subsequent high temperature ageing. Five repaired pipe mock-ups were manufactured: a general arrangement of a completed mock-up is shown in Figure 5, and full details are recorded elsewhere [29].

4 Residual stress measurements

4.1 As-welded condition

Residual stress measurements were made using both incremental deep hole drilling (iDHD) [30], and the contour method [31, 32].

A single iDHD measurement was made on a through-wall line on the weld centreline of pipe CY5/CY9, remote from the start/stop positions of the capping beads, see Figure 2. This measurement recovered hoop and axial stresses. A second through-wall measurement, also visible in Figure 2, was made in parent material ~50mm from the weld centreline. Both measurements produced some anomalous results. The weld centreline measurement was found to have passed through the lack of fusion defect at the weld root, which introduced a crack into the trepanned core extracted from the pipe. Data close to the inner wall from this measurement were thus discarded, since the presence of a weld defect invalidates the assumptions used to calculate stresses from changes in diameter of the initial gun-drilled hole. The parent material measurement also produced unexpected results, which agreed neither with the quench stress profiles predicted from modelling, nor with subsequent contour method measurements. No results from this measurement are presented.

Two contour method measurements were made on pipe CY7/CY6. These are described more fully elsewhere [31-33]. The first measurement was made in an axial plane on the axis of the pipe, and simultaneously revealed the full field hoop stress distribution in the pipe on two axial-radial planes 180° apart, see Figure 6. The second measurement was made on a

transverse plane on the weld centreline of one of the remaining half pipes. This revealed the axial stress distribution over the half pipe, see Figure 6.

Hoop stresses measured by the two techniques on a through-wall line at the weld centreline are compared in Figure 7. The iDHD measurements are not plotted for the first 20% of the cross-section to eliminate the errors caused by the weld root defect at the inner wall. Contour method measurements are presented for two lines 180° apart. The peak stresses measured by the two techniques agree closely at about 450 MPa, beneath the outer surface, with similar through-wall profiles.

Comparing axial stresses is more complicated, as the contour method measurement recovers a large amount of data in the form of a map over half the circumference of the pipe (see Figure 6). Figure 8 plots the through-wall distributions of axial stress measured at 15° intervals around the half-section of pipe CY7/CY6. It can be seen that the stresses do vary with position. This is not unexpected – as a minimum, the start/stop effects associated with the capping passes will generate non-axisymmetric stresses in a pipe girth weld. Figure 8 also plots a sixth-order polynomial fit to all the individual through-wall profiles. This profile has a membrane stress component very close to zero. Zero average membrane stress is the expected outcome for this pipe geometry, so achieving this gives confidence in the general accuracy of the contour measurements. The iDHD measurement made on pipe CY5/CY9 is also plotted on Figure 8. This falls within the range of the contour method results, with a peak stress below the outer surface close to the upper bound of the contour data. It should be noted that the iDHD measurement was made on a weld with three capping passes, with the final pass in the centre of the weld, while the contour measurements were made on a weld with two capping passes. The simulations described in Part 2 of this study indicate that a central capping pass is expected to produce peak axial stresses about 50 MPa higher on the weld centreline than an offset capping pass, so the magnitude of the iDHD peak is no surprise, despite the measurement being remote from the stop location of the final capping pass.

4.2 After high temperature exposure

A single through-wall DHD measurement was made on the weld centreline of pipe CY10/CY8 after ageing for 10,000 hours at 650°C. The hoop stresses are compared with those measured after welding in Figure 7, and the axial stresses in Figure 9. Considerable stress relaxation has occurred, with peak stresses in both directions only slightly higher than 100 MPa.

Both DHD and contour method measurements were also made on long pipes containing repairs after ageing, in both cases after 20,000 hours at 650°C [30, 34]. The additional time at

temperature is expected to result in little further stress relaxation beyond that observed after 10,000 hours, based upon the modelling reported in Part 2 of this study. The measurements in the girth welds of the long pipes were judged to be equivalent to those made in the short pipe, so are reproduced here for comparison.

The measured hoop stresses are plotted on Figure 7. The long pipe measurements agree closely with the short pipe measurements, except very close to the outer wall, where the DHD measurement in the long pipe rises somewhat. The reason for this is not clear. Both measurement techniques show greater uncertainty close to the surface, although the deviation occurs at depths greater than those normally censored from DHD measurements.

The measured axial stresses are plotted on Figure 9. Here the DHD measurements made on the long and short pipes show larger differences. However, reference to Figure 8 shows that some circumferential variation in axial stress is expected even in a plain girth weld.

5 Materials characterization

Austenitic stainless steels exhibit significant work hardening in weld metal and in the adjacent heat/strain affected zone as a result of the thermo-mechanical cyclic loading induced by welding [35]. It has been shown [13, 36-38] that the most accurate predictions of the development of weld residual stresses in these steels are made using mixed isotropic-kinematic hardening models, which allow the yield surface both to expand and translate. Esshete 1250 is expected to show similar behaviour to more common steels like the AISI 316L studied by the NeT network.

The mechanical properties of both Esshete 1250 parent material and the matching Esshete 1250 MMA weld metal were characterized in a programme funded by British Energy (now EDF Energy) and performed by Serco Assurance (now Wood Group) [27]. Both monotonic and isothermal cyclic tests were performed over a range of temperatures from room temperature up to 1000°C for tensile tests, and 700°C for cyclic tests. The complete test matrix is presented in Table 1.

5.1 Parent material testing

Parent material for testing was extracted from near mid-thickness of one of the long pipe sections made from the same piece of Esshete 1250 bar and described above. The mid-thickness location was chosen to minimize quench-induced plastic strain. All test specimens were extracted in the pipe longitudinal direction.

The test parameters were consistent with the advice given in R6 [3, 6]. A single strain rate of $4\times10^{-4}s^{-1}$ was used for all testing. This is close to the strain rates expected during the later

stages of cooling, when the material has significant strength and the final tensile residual stress field is developing close to the weld. Little strain rate sensitivity is expected for this material over the test temperature range. The choice of strain range for cyclic tests is more complex. Welding generates asymmetric plastic strain cycles in adjacent parent and HAZ material, with the majority of the plastic strain developing in compression during heating (see [13]). The average strain range per weld pass also varies with distance from the weld bead, and in multi-pass welds it tends to decrease as successive passes are laid down [39]. There is a practical upper limit of about 3% to the strain range that can be applied in a cyclic test on austenitic steels without frequent specimen buckling. R6 recommends that parent material be tested at 2.5% or greater total strain range. Here, the majority of tests were performed at a lower TSR of 1.5%, with supplementary testing at 2.5% TSR at three temperatures, see Table 1.

5.2 Weld metal testing

Deriving a mixed hardening model for weld metal is more challenging than for parent material. In the real structure, weld metal is introduced molten and cyclically hardens under the thermo-mechanical loading associated with initial cool-down and the deposition of subsequent weld beads. A completed multi-pass weld will therefore exhibit a gradient of yield strength from the weld root to the weld cap, with the highest yield strength at the root, where both the plastic path length and the number of thermo-mechanical cycles are greatest, and the lowest in the last capping pass, where the plastic path length is shortest and the material has experienced a single cooldown quarter cycle from molten.

This trend is confirmed by Vickers Hardness measurements made on a transverse cross-section of the two-capping-pass weld in pipe CY7/CY6, see Figure 10. These show a marked gradient in hardness, rising from ~178 kgf/mm^2 in the final capping pass to ~285 kgf/mm^2 in the weld root. As hardness is approximately proportional to yield strength, this implies that the yield strength in the root is about 1.6x that of the final capping pass.

Multi-pass weld metal is clearly unsuitable for testing to derive evolutionary hardening models in its as-welded state. The material used for testing to develop mixed hardening parameters for weld metal must start in a state that is a reasonable facsimile of “just-deposited”, unhardened weld metal. The test programme examined two weldment types and two heat treatment conditions. A small number of monotonic tensile test specimens were extracted from a multi-pass pipe girth weld identical to those considered here, made with the same batch of consumables and following the same welding procedure. These were tested in the as-received condition. All the remaining specimens were extracted from single pass MMA welds laid into grooves, again using the same batch of consumables. This weld

configuration was expected to contain very little cyclic hardening, and thus be close to "as-deposited" material. The majority of the single pass specimens were tested in the as-received condition. A small number underwent a "spike annealing" heat treatment, where the specimen was rapidly heated to 850°C or 950°C in an induction coil, and then allowed to cool in air, to simulate the thermal effect of depositing an adjacent bead. Monotonic tensile tests were performed on all three specimen conditions at room temperature. Elevated temperature tensile testing was performed on single pass weld metal with no final thermal treatment, up to a peak temperature of 1000°C.

Isothermal cyclic tests were performed at a single total strain range (TSR) of 1.5%, up to a peak temperature of 700°C, only on single pass weld metal with no final thermal treatment.

5.3 Monotonic and cyclic test results

Figure 11 presents the isothermal cyclic stress-strain responses of both parent material and weld metal at room temperature, as follows:

- Figure 11a: two 1.5% TSR tests on parent material
- Figure 11b: three 1.5% TSR tests on single-pass weld metal
- Figure 11c: comparison of parent material and weld metal at 1.5% TSR
- Figure 11d: the effect of strain range on the response of parent material

The 1.5% TSR tests are plotted at cycle 1, cycle 3, and cycle 14. Cycle 14 corresponds broadly to cyclic saturation. The 2.5% TSR tests saturate faster, as would be expected from their higher strain range, and results for this test condition are plotted at cycles 1, 2, 3, and 10.

Both parent and single pass weld metal initially cyclically harden rapidly, and they achieve saturation by cycle 14 at 1.5% TSR. Their responses are qualitatively very similar, although weld metal has a higher initial yield strength, and shows more specimen to specimen variation. Increasing the strain range increases the amount of cyclic hardening, as expected.

Figure 12plots the temperature dependence of the both the 0.2% proof stress on first loading, and the yield strength at cyclic saturation, for parent material, as follows:

- The 0.2% proof stress for all tests, both tensile and cyclic
- The cyclically saturated yield strength at 1.5% TSR (mint circles) and at 2.5% TSR (mint triangles)

- The isotropic hardening limit, Q_{inf}, at 1.5% TSR (yellow circles), and at 2.5% TSR (yellow triangles)[1]

As expected, the initial yield strength decreases with increasing temperature. In contrast, the extent of cyclic hardening increases with increasing temperature, peaking at about 400°C, before falling sharply above 600°C. Increasing the strain range increases both Q_{inf} and the cyclically saturated yield strength at all temperatures, although the effect at 400°C is modest.

Figure 13 compares the same data for parent material and single-pass weld metal tested under identical conditions. The two materials show very similar trends in behaviour. The only significant difference is the higher 0.2% proof stress of weld metal. This is not surprising: single pass weld metal will contain ~1-2% of accumulated plastic strain, which will raise its yield strength.

Studies performed on AISI 316L weld metal and reported by the NeT network [40] have shown that its yield strength depends strongly upon the state of the weld metal being tested. The testing on Esshete 1250 reported here covers a much smaller variation in weld metal conditions. Figure 14 compares the measured 0.2% proof stress for single-pass Esshete 1250 weld metal with the following:

- The 0.2% proof stress measured for multi-pass Esshete weld metal in this study at room temperature
- The mean 0.2% proof stress of multi-pass Esshete weld metal extracted from a number of weldments, measured over a range of temperatures, from a large internal study at EDF Energy [41]
- The 0.2% proof stress of material extracted from passes 1 and 3 of a three-pass MMA weld laid into a groove in Esshete 1250, measured using electron speckle-pattern interferometry (ESPI) techniques on cross-weld specimens [42]
- The mean 0.2% proof stress of multi-pass AISI 316L weld metal extracted from a number of weldments, measured over a range of temperatures, from a large internal study at EDF Energy [43]
- The measured 0.2% proof stress of "spike-annealed" single pass AISI 316L MMA weld metal [40]

---

[1] Q_{inf} is the difference between the peak tensile stress achieved in the first quarter cycle, and the peak tensile stress reached at saturation at the same strain level.

- The measured 0.2% proof stress of solution-treated 2-pass AISI 316L TIG weld metal[2] [40].

The 0.2% proof stress of single pass Esshete weld metal is very similar to that of equivalent spike-annealed AISI 316L material. The spike annealing heat treatment slightly reduced the yield strength of AISI 316L whereas it had no discernible effect on Esshete 1250. Both Esshete and AISI 316L single pass weld metal have a significantly higher yield strength than solution treated AISI 316L. The latter specimens are completely free of work hardening, whereas the non-heat-treated specimens are not.

The transverse yield strength of the final pass of a three-pass Esshete weld measured using ESPI is also close to that measured in the longitudinal direction of single pass welds. This is consistent with the levels of accumulated plastic strain in the two welds, which are expected to be about the same.

The yield strength of multi-pass Esshete 1250 weld metal is significantly higher than that of AISI 316L (a ratio of 1.3x at room temperature). It is also evident from the ESPI data that pass 1 of a three-pass weld, which has undergone 2.5 thermo-mechanical load cycles, has already hardened to close to the multi-pass yield strength.

Figure 15 compares the cyclic saturation limit measured for Esshete 1250 single pass weld metal with both the ESPI cross-weld test results and the mean 0.2% proof stress of multi-pass weld metal. The expectation is that cyclic saturation should correspond to the measured yield strength of multi-pass weld metal, since this is the end state of the thermo-mechanical cycling that takes place during welding. At temperatures of 400°C and above, this is indeed the case. However below 400°C the cyclic saturation limit is well below the yield strength of multi-pass weld metal. At room temperature it does not even reach that of pass 1 in a three-pass weld.

What are the implications of these observations for parameter fitting of mixed hardening models?

Experience with AISI 316L and AISI 316L(N) in the NeT TG1 and TG4 projects has shown that fitting to data from non-heat-treated single pass weld metal tests leads to a significant over-estimate of the stresses in the final deposited weld pass [36, 37], because the initial yield strength is too high. Fitting to data from solution-treated "single pass" material, which contains no prior plastic strain, leads to much more accurate predictions of stress [40]. The

---

[2] Note that the first weld pass in these specimens was almost completely re-melted, so they are effectively single-pass welds.

same will be true for Esshete 1250. However, the importance of this depends on the geometry of the weldment being modelled. The NeT benchmarks contain few weld passes, so the final weld bead occupies a significant proportion of the weld. The final bead in a multi-pass pipe girth weld is likely to be a much smaller proportion of the weld, so errors in the initial yield strength may be less important if the weld metal cyclically hardens fast. The potential underestimate of the final yield strength of multi-pass welds is of more concern for a multi-pass weld. R6 [3, 6] recognizes this and requires that mixed hardening models for weld metal should harden to the multi-pass weld metal yield strength. *Both these issues are addressed in the parameter-fitting strategies adopted in this study.*

6 Mixed isotropic-kinematic model parameter fitting

The Lemaitre-Chaboche model [44] is often used to represent mixed hardening. As implemented in the ABAQUS FE code [45], the isotropic and non-linear kinematic parts of a cyclic hardening model are described separately. The kinematic hardening component describes translation of the yield surface in stress space via the backstress tensor $\boldsymbol{\alpha}$. The pressure-independent yield surface f is defined by the function:

$$f(\boldsymbol{\sigma}-\boldsymbol{\alpha}) = \sigma^0 \qquad (1)$$

where $\boldsymbol{\sigma}$ is the stress tensor, σ^0 is the radius of the yield surface and $f(\boldsymbol{\sigma}-\boldsymbol{\alpha})$ is the equivalent von Mises stress, defined by:

$$f(\sigma-\alpha) = \sqrt{\frac{3}{2}(\mathbf{S}-\alpha^{dev}):(\mathbf{S}-\alpha^{dev})} \qquad (2)$$

here $\boldsymbol{\alpha}^{dev}$ is the deviatoric part of the back stress tensor, and $\mathbf{S}$ is the deviatoric stress tensor, defined as $\mathbf{S}=\boldsymbol{\sigma}+p\mathbf{I}$, where p is the equivalent pressure stress, and $\mathbf{I}$ is the identity tensor.

The kinematic hardening component is defined as an additive combination of a purely kinematic term (the linear Ziegler hardening law) and a relaxation term (the recall term), which introduces nonlinearity. When temperature and field variable dependencies are omitted, the kinematic hardening law is:

$$\dot{\boldsymbol{\alpha}} = \sum_i \left[C_i \frac{1}{\sigma^0}(\boldsymbol{\sigma}-\boldsymbol{\alpha})\dot{\bar{\varepsilon}}^{pl} - \gamma_i \boldsymbol{\alpha}\dot{\bar{\varepsilon}}^{pl} \right] \qquad (3)$$

where C_i and γ_i are material parameters that must be calibrated from monotonic or cyclic test data. C_i is the initial kinematic hardening modulus, and γ_i determines the rate at which the

kinematic hardening modulus decreases with increasing plastic deformation. $\boldsymbol{\sigma}$ is the stress tensor, σ^0 , is the equivalent stress defining the size of the yield surface, and $\dot{\bar{\varepsilon}}^{pl}$ is the equivalent plastic strain rate. Only the deviatoric part of $\boldsymbol{\alpha}$ contributes to the material hardening behaviour. When C_i and γ_i are both zero, the model reduces to pure isotropic hardening.

The isotropic hardening component of the model defines the evolution of the yield surface size, σ^0, as a function of the equivalent plastic strain, or plastic path length, $\bar{\varepsilon}^{pl}$.

$$\sigma^0 = \sigma|_0 + Q_{inf}\left(1 - e^{-b\bar{\varepsilon}^{pl}}\right) \qquad (4)$$

where $\sigma|_0$ is the yield stress at zero plastic strain, and Q_{inf} and b are material parameters. Q_{inf} is the maximum change in the size of the yield surface, and b defines the rate at which the size of the yield surface changes as plastic straining develops. When the equivalent stress defining the size of the yield surface remains constant ($\sigma^0 = \sigma|_0$), the model reduces to pure kinematic hardening.

The Lemaitre-Chaboche model is designed primarily to model cyclic inelastic loading of metals, where the cyclic load is imposed either mechanically or thermally. The mixed isotropic-kinematic formulation allows the model to describe both the Bauschinger effect, where the yield is reduced upon load reversal after plastic deformation during initial loading, and cyclic hardening with plastic shakedown, where soft or annealed metals tend to harden towards a stable limit during cyclic loading.

The model has the advantage of being computationally robust, with a minimum of five fitting parameters at each temperature, which can all be derived from the results of simple monotonic tensile and uniaxial cyclic tests. However, it retains limitations when applied to complex loading over a wide temperature range, due to the nature of its implementation within finite element codes. These include:

1. The isotropic hardening parameters Q_{inf} and b can only be fitted to tests performed at a single strain range, and are then applied to all strain ranges. In practice the amount of cyclic isotropic hardening varies with the strain range used for testing, and it tends to increase with increasing strain range. The strain range chosen for cyclic testing and parameter fitting must therefore be representative of the strain ranges expected in the real structure.
2. The kinematic parameters C_i and γ_i cannot vary with strain range, and they are used to describe both the monotonic and cyclic response of the material. This can lead to difficulties in matching both the monotonic and cyclic response. The most important

features of the expected structural loading must therefore be understood and the fit optimised to model these features correctly.

3. Although γ_i can vary with temperature, in practice convergence difficulties are often encountered unless it is fixed over the full range of temperature. Fixing γ_i is normally a reasonable assumption for austenitic steels.
4. The model is calibrated using the results of isothermal uniaxial tests, where the loading is proportional (the principal stress axes do not rotate). The actual hardening behaviour of a material during a thermo-mechanical fatigue cycle (TMF loading) or under non-proportional loading may differ from that in an isothermal uniaxial test.
5. Equivalent plastic strain is accumulated within the model with no regard for temperature. Thus an increment of equivalent plastic strain accumulated at a high temperature may lead to a small increment in yield strength at that temperature. However, if the temperature falls to room temperature, that increment of equivalent plastic strain is deemed to have led to the much larger increment in yield strength that would occur had the same strain been accumulated at room temperature.

The kinematic parameters C_i, γ_i, and $\sigma|_0$ are normally fitted first. Here it is necessary to decide whether it is more important to match the monotonic or the cyclic response.

The best fit to the saturated cyclic response is obtained by fitting C_i and γ_i to the shape of the saturated cyclic stress-strain loop from a symmetric strain-controlled isothermal cyclic test. This procedure will naturally yield the "best" stress-strain loop shape for the strain range of the test used for fitting. However, it has the following drawbacks:

1. It normally does not predict the monotonic response well. The model is usually too "soft", with the proportional limit stress too low, and insufficient work hardening beyond the peak strain of the cyclic test used for fitting.
2. The fitted parameters do not normally lend themselves to extrapolation to higher cyclic strain ranges, since the hardening slope beyond the peak fitted strain is often too low.

An alternative is to fit C_i, γ_i, and $\sigma|_0$ to the monotonic response of the material, derived from tensile tests which extend up to a suitable maximum plastic strain. Integration of the back-stress evolution law of Equation (3) over a half cycle yields the relationship:

$$\sigma = \sigma|_0 + \sum_i \left[\frac{C_i}{\gamma_i} (1 - \exp(-\bar{\varepsilon}^{pl} \gamma_i)) \right] \qquad (5)$$

Equation (5) may be fitted to the monotonic true stress vs. plastic strain response of the material up to the chosen peak plastic strain, the magnitude of which depends on both the

expected peak monotonic strain excursion expected in the structure, and the need to produce acceptable cyclic stress-strain loop shapes. Clearly, when fitting multi-temperature datasets with the constraint of constant γ_i over temperature, care must be also taken to optimise the overall fit.

A compromise approach has been adopted for the NeT TG4 benchmark, in which Equation (5) is fitted to the response during the first re-loading into tension. This has the advantage of improving the representation of the Bauschinger effect, at the expense of a slight reduction in the initial monotonic yield strength.

Once the kinematic parameters have been chosen, then fitting Equation (4) is relatively straightforward. The parameter Q_{inf} is obtained from cyclic test data with an appropriate strain range: it is the difference between the peak stress at peak positive strain in the first quarter cycle in the cyclic test (from Equation (5)), and half the total stress range $\Delta\sigma/2$, either at saturation or at a cycle number deemed appropriate. The hardening rate parameter b is then fitted to achieve an appropriate hardening rate.

6.1 Parent material models

The most extensive data set available for Esshete 1250 parent material was generated at 1.5% TSR. Testing was performed at 2.5% TSR only at selected temperatures. R6 recommends that parameter fitting be performed on tests conducted at 2.5% TSR or greater, in order to bound the cyclic hardening response of the entire HAZ region [3]. To achieve this, the following procedure was followed:

1. The kinematic parameters were fitted to data from the monotonic tensile tests and the 1.5% TSR tests
2. The cyclic isotropic parameters were initially fitted to the 1.5% TSR tests
3. The cyclic hardening limit Q_{inf} was then increased at all temperatures to ensure that the fitted model parameters acceptably represented the 2.5% TSR tests.

Three kinematic parameter fits were performed:

1. The first, effectively a historical fit (see [39]), used a single C, γ pair, that is a single back-stress, at each temperature, fitted to monotonic test data up to 5% plastic strain. Because a single C, γ pair is insufficient to fully represent the work hardening behaviour of an austenitic steel, the strain range of the fit was a compromise to obtain acceptable monotonic and cyclic behaviour.
2. The second used two C, γ pairs, ie two back-stresses, at each temperature to reproduce the monotonic response. Two C, γ pairs are sufficient to reproduce the

monotonic work hardening behaviour of this steel without any need to tune the fitting range.

3. The third used two C, γ pairs at each temperature to reproduce the first reloading into tension in a cyclic test.

The fitted parameters are reproduced in Table 2, Table 3 and Table 4. The predicted room temperature responses of the three kinematic parameter fitting strategies are compared with both monotonic tensile and 1.5% TSR cyclic tests in Figure 16. Note that the historical single C, γ fit includes adjustments to better match 2.5% TSR tests, while the two two-back-stress fits do not incorporate these adjustments. The pattern revealed by Figure 16 is similar to that observed for AISI 316L: the two back-stress monotonic fit matches first loading extremely well, at the expense of a weakened Bauschinger effect, while the two back-stress cycle 2 fit accurately reproduces the cyclic response at the expense of underestimating the monotonic yield strength. The historical single C, γ fit is a surprisingly good compromise to both monotonic and cyclic responses at this strain range.

Figure 17 illustrates the application of the fitted back-stress models to room temperature 2.5% TSR tests. In both cases Q_{inf} is adjusted to correctly predict cyclic saturation. It is noteworthy that the monotonic fit seems to extrapolate to higher strain ranges better than the cycle 2 fit.

6.2 Weld metal models

The fitting of an Esshete weld metal model has two additional complications over a parent material model:

1. Ensuring that the cyclic hardening limit is sufficient to achieve the yield strength of multi-pass weld metal at saturation
2. Making adjustments to the initial yield strength to account for the presence of prior work hardening in the weld metal that has been tested.

The same three fundamental assumptions were made in fitting the kinematic model parameters:

- a single back stress at each temperature, fitted to monotonic test data up to 2% plastic strain.
- two back stresses at each temperature to reproduce the monotonic response.
- two back stresses at each temperature to reproduce the first reloading into tension in a cyclic test.

The three parameter sets were first fitted to a combination of monotonic and 1.5% TSR cyclic tests, with Q_{inf} and b fitted to match the unadjusted cyclic test data. A number of modifications were then made to the fitted models:

- To adjust the hardening limit Q_{inf} to ensure fully hardened weld metal reached the mean 0.2% proof stress of multi-pass Esshete weld metal (the R6 recommendation).
- To reduce the initial yield strength by reducing σ_0, to simulate as-deposited weld metal with no accumulated plastic strain.
- To change the cyclic hardening rate.

The full set of fitted models are listed in Table 5.

7 Conclusions

A number of engineering scale multi-pass pipe girth weld mock-ups have been manufactured using conventional manual metal arc techniques from Esshete 1250 austenitic steel, with the welding process characterised in detail in order to provide validation benchmarks for finite element prediction of weld residual stresses.

1. Contour method measurements of hoop stress made in the as-welded condition reveal quench stresses remote from the weld, compressive at the surface and tensile in the bulk of the material, and typical weld residual stress distributions at the weld, with tensile peak stresses beneath the last capping pass and compressive stresses near the inner bore.
2. Hoop residual stresses measured on the weld centreline using incremental deep hole drilling and the contour method agree closely: tensile stresses peak below the outer surface at about 450 MPa, and compressive stresses reach about -400 MPa near the inner bore.
3. Contour method measurements of axial stress on the weld centreline reveal circumferential variation in the as-welded through-wall profiles, although the mean membrane stress is close to zero, as expected for an axisymmetric weld.
4. Contour and iDHD measurements of axial stress show good general agreement, with a sinusoidal through-wall distribution, and both tensile and compressive peak stresses between +/- 200 – 300 MPa.
5. Hardness mapping made in the as-welded condition reveals significant hardening in both weld and adjacent HAZ material, with an overmatched weld. The measured through-wall hardness gradient is consistent with little work hardening in the last capping pass, a significant increase in work hardening in material that has seen ~1.5 thermo-mechanical cycles, and thereafter a steady rise as the weld root is approached.

The hardness measurements are consistent with a 1.6X increase in yield strength between last capping pass and weld root.

6. High temperature exposure for 10,000 and 20,000 hours at 650°C causes significant reductions in residual stress. Both hoop and axial stresses reduce to slightly more than 100 MPa.
7. Monotonic tensile testing performed between ambient temperature and 1000°C on parent metal and single pass MMA weld metal (which contains some plastic strain) reveals room temperature 0.2% proof stresses of ~290 MPa for parent material, and ~335 MPa for weld metal, with steady decrease with increasing temperature up to ~700°C and a rapid fall thereafter. The 0.2% proof stress of multi-pass Esshete 1250 weld metal (its hardened end state) is much higher, at ~560 MPa at room temperature.
8. The testing of multi-pass weld metal is not appropriate for the development of evolutionary mixed hardening models. Single pass weld metal is much better, but still contains some work hardening, meaning its initial yield strength is still slightly too high.
9. Both parent and weld metal cyclically harden rapidly, achieving saturation after ~14 cycles at 1.5% TSR for both forms, and after ~10 cycle at 2.5% TSR for parent material. More hardening takes place at higher strain ranges.
10. Weld metal does not cyclically harden to the yield strength of multi-pass weld metal at low temperatures, but does above 400°C. This suggests that the thermo-mechanical response of the material cannot be derived solely from isothermal testing.
11. The non-linear kinematic portion of the Lemaitre Chaboche hardening model cannot simultaneously match the monotonic and cyclic responses of Esshete 1250. Kinematic model parameters for weld simulation were thus derived using three assumptions: fitting two back-stresses to the monotonic response, fitting two back-stresses to the first reloading into tension, and a “legacy” single back-stress fit to the monotonic response.
12. The cyclic isotropic hardening response of parent models was fitted to ensure adequate hardening at high strain ranges, using both 1.5% and 2.5% TSR test data.
13. The fitted parameter sets for weld metal were derived using similar assumptions for the kinematic response. In addition, the initial proportional limit stress was reduced to account for the unwanted strain hardening already present in the weld metal tested, the cyclic hardening limit was increased to ensure that the fitted models hardened to the measured yield strength of multi-pass weld metal, and the cyclic hardening rate was varied to examine the impact of different hardening rates at different temperatures.

8 Acknowledgments

The work reported here is a collaborative effort spread over a number of organisations. The authors are grateful to all the participants in the STYLE Framework 7 project. Particular thanks are due to the late Professor David Smith, of the University of Bristol. David led the residual stress research activities within STYLE, particularly the deep hole drilling residual stress measurements. He is greatly missed by his colleagues.

Mike Smith and Qingrong Xiong are supported via the EPSRC Fellowship in Manufacturing "A whole-life approach to the development of high integrity welding technologies for Generation IV fast reactors", EP/L015013/1.

This paper is published with the permission of EDF Energy.

9 References

1 L-E Lindgren, Computational welding mechanics. Thermomechanical and microstructural simulations, Cambridge, Woodhead Publishing Ltd (2007).
2 L-E Lindgren, Finite element modeling and simulation of welding part 2: improved material modelling, J Therm Stress **24**, 195-231 (2001).
3 R6, Assessment of the integrity of structures containing defects, EDF Energy (2015).
4 Fitness for Service, API 579-1/ASME FFS-1, Second Edition (2007).
5 P Hurrell, C Watson, P J Bouchard, M C Smith, R J Dennis, N A Leggatt, S K Bate and A Warren, Development of weld modelling guidelines in the UK, ASME PVP 2009, Prague, PVP2009-77540 (2009).
6 S Bate and M Smith, Determination of residual stresses in welded components by finite element analysis, Materials Science and Technology **32**(14), 1505-1516 (2016).
7 C Ohms, R V Martins, O Uca, A G Youtsos, P J Bouchard, M C Smith, M Keavey, S K Bate, P Gilles, R C Wimpory and L E Edwards, The European network on Neutron Techniques Standardization for Structural Integrity - NeT 2008 ASME Pressure Vessels and Piping Division Conference, Chicago, PVP2008-61913 (2008).
8 M C Smith, A C Smith, R C Wimpory, C Ohms, B Nadri and P J Bouchard, Optimising residual stress measurements and predictions in a welded benchmark specimen: a review of Phase two of the NeT Task Group 1 single bead on plate round robin, 2009 ASME Pressure Vessels and Piping Division Conference, Prague, 26th-30th July 2009, PVP2009-77157 (2009).
9 P J Bouchard, The NeT bead on plate benchmark for weld residual stress simulation, Int Jnl Press Vess and Piping **86**(1), 31-42 (2009).
10 C E Truman and M C Smith, The NeT residual stress measurement and analysis round robin on a single weld bead-on-plate specimen, Int Jnl Press Vess and Piping **86**(1), 1-2 (2009).
11 M C Smith and A C Smith, NeT bead on plate round robin: Comparison of transient thermal predictions and measurements, Int Jnl Press Vess and Piping **86**(1), 96-109 (2009).
12 M C Smith and A C Smith, NeT bead on plate round robin: Comparison of residual stress predictions and measurements, Int Jnl Press Vess and Piping **86**(1), 79-95 (2009).
13 O Muransky, M C Smith, P J Bendeich, T M Holden, V Luzin, R V Martins and L Edwards, Comprehensive numerical analysis of a three-pass bead-in-slot weld and its critical validation using neutron and synchrotron diffraction residual stress measurements, International Journal of Solids and Structures **49**(9), 1045-1062 (2012).
14 M C Smith, S K Bate and P J Bouchard, Simple benchmark problems for finite element weld residual stress simulation, ASME Pressure Vessels and Piping Conference, Paris, PVP2013-98033 (2013).
15 S Marlette, P Freyer, M C Smith, A Goodfellow, X Pitoiset, B Voigt, R Rishel and E J Kingston, Simulation and measurement of through-wall residual stresses in a structural weld overlaid pressurizer nozzle, ASME PVP 2010, Bellevue, WA, July 18-22 2010, PVP2010-25736 (2010).

16 M C Smith, O Muransky, P J Bendeich and L Edwards, The impact of key simulation variables on predicted residual stresses in pressuriser nozzle dissimilar metal weld mock-ups. Part 1 – simulation, ASME PVP 2010, Bellevue, Wa, July 18-22 2010, PVP2010-26023 (2010).
17 M C Smith, O Muransky, A Goodfellow, E J Kingston, P Freyer, S Marlette, G Wilkowski, F Brust and D J Shim, The impact of key simulation variables on predicted residual stresses in pressuriser nozzle dissimilar metal weld mock-ups. Part 2 – comparison of simulation and measurements, ASME PVP 2010, Bellevue, Wa., 18-22 July 2010, PVP2010-26025 (2010).
18 O Muransky, M C Smith, P J Bendeich and L Edwards, Validated numerical analysis of residual stresses in Safety Relief Valve (SRV) nozzle mock-ups, Computational Materials Science **50**(7), 2203-2215 (2011).
19 P J Bendeich, O Muransky, C J Hamelin, M C Smith and L Edwards, Validated numerical analysis of residual stresses in safety relief valve (SRV) nozzle mock-ups: influence of axial restraint on distortion and residual stress predictions, Computational Materials Science **62**, 285-288 (2012).
20 H J Rathbun, D Rudland, L Fredette, A Csontos and P Scott, NRC welding residual stress validation program – International round robin details and findings, 2011 ASME Pressure Vessels and Piping Division Conference, Baltimore, 17th-20th July 2011, PVP 2011-57642 (2011).
21 L Fredette, M Kerr, H J Rathbun and J E Broussard, NRC/EPRI Welding Residual Stress Validation Program - Phase III Details and Findings, ASME Pressure Vessels and Piping Conference, Baltimore, PVP2011-57645 (2011).
22 P J Bouchard, Validated residual stress profiles for fracture assessments of stainless steel pipe girth welds, Int Jnl Press Vess and Piping **84**(4), 195-222 (2007).
23 D J Smith, P J Bouchard and D George, Measurement and prediction of residual stresses in thick-section steel welds, The Journal of Strain Analysis for Engineering Design **35**(4), 287-305 (2000).
24 A H Mahmoudi, S Hossain, C E Truman, D J Smith and M J Pavier, A new procedure to measure near yield residual stresses using the deep hole drilling technique, Experimental Mechanics **49**(4), 595-604 (2008).
25 M B Prime, Cross-Sectional Mapping of Residual Stresses by Measuring the Surface Contour After a Cut, Journal of Engineering Materials and Technology **123**(2), 162-168 (2000).
26 M C Smith, A C Smith and T Nicak, Final Report of the STYLE project, European Commission Seventh Framework Programme Report (2014).
27 C Austin and L A Higham, A Constitutive Model for Parent Esshete 1250 and Associated Single Bead Weld Metal, Serco Assurance Report SA/SIA/17261/R01, Issue 1 (2008).
28 M C Smith and A C Smith, Advances in weld residual stress prediction: A review of the NeT TG4 simulation round robin part 1, thermal analyses, Int Jnl Press Vess and Piping, (2017).
29 R L Jones and D Bertaso, Manufacture of Esshete Repair Welded Pipe Test Specimens, TWI Report 15709/1/05 (2005).
30 S Do, D J Smith and M C Smith, Effect of Ageing on Residual Stresses in Welded Stainless Steel Cylinders, ASME Pressure Vessels & Piping Conference, Toronto, Ontario, Canada, PVP2012-78528 (2012).
31 J Mathew, R J Moat and P J Bouchard, Prediction of Pipe Girth Weld Residual Stress Profiles Using Artificial Neural Networks, ASME Pressure Vessels and Piping Conference, Paris, July 14-18 (2013).
32 J Mathew, R J Moat, S Paddea, J A Francis, M E Fitzpatrick and P J Bouchard, Through-Thickness Residual Stress Profiles in Austenitic Stainless Steel Welds: A Combined Experimental and Prediction Study, Metallurgical and Materials Transactions A **48**(12), 6178-6191 (2017).
33 J Mathew, R J Moat, S Paddea, M E Fitzpatrick and P J Bouchard, Prediction of residual stresses in girth welded pipes using an artificial neural network approach, Int Jnl Press Vess and Piping **150**, 89-95 (2017).
34 S Paddea, Residual stress measurement of a repaired Esshete pipe girth weld after heat soak, The Open University Report (2015).
35 M Turski, M C Smith, P J Bouchard, L Edwards and P J Withers, Spatially resolved materials property data from a uniaxial cross-weld tensile test, Journal of Pressure Vessel Technology **131**(6), (2009).
36 M C Smith and A C Smith, Advances in weld residual stress prediction: a review of the NeT TG4 simulation round robin part 2, mechanical analyses, Int Jnl Press Vess and Piping **Special Issue in memory of Ann Smith**, (2018).
37 M C Smith, A C Smith, R Wimpory and C Ohms, A review of the NeT Task Group 1 residual stress measurement and analysis round robin on a single weld bead-on-plate specimen, Int Jnl Press Vess and Piping **120–121**(0), 93-140 (2014).

38 M C Smith, P J Bouchard, M Turski, L Edwards and R J Dennis, Accurate prediction of residual stress in stainless steel welds, Computational Materials Science **54**, 312-328 (2012).
39 M C Smith, Development of mixed isotropic-kinematic material hardening models for finite element simulation of austenitic steel welds, British Energy Report E/REP/BDBB/0092/AGR/06, Revision 000 (2006).
40 M C Smith, O Muransky, C Austin and P J Bendeich, Optimised modelling of AISI 316L(N) material behaviour in the NeT TG4 international weld simulation and measurement benchmark, Int Jnl Press Vess and Piping **Special Issue in memory of Ann Smith**, (2017).
41 J P Douglas, Review of Available Tensile Data for Parent and Weld Esshete Stainless Steel, Frazer-Nash Consultancy Report FNC 32213-001-05/52182TN, Issue 2 (2006).
42 S Ganguly, Boiler Spine Residual Stress Measurements Programme Task 2.2: Cross-weld tensile tests of 3-pass Esshete circular plate groove weld, The Open University Report OU/BE/BoilerSpineTask2.2/EssheteESPI (2008).
43 J P Douglas, Review of Available Tensile Data for Parent and Weld 316 Stainless Steel, Frazer-Nash Consultancy Report FNC 32213-001-05/52165TN, Issue 2 (2006).
44 J Lemaitre and J L Chaboche, Mechanics of Solid Materials, Cambridge University Press (1990).
45 ABAQUS/Standard User's Manual, Version 6.9, Providence, RI, Simulia (2009).

10Tables

Table 1: Mechanical test programme for Esshete 1250 parent material and weld metal [27]

Material	Condition	Test Type	Temperatures	Strain range	Orientation
Parent	As-received	Uniaxial tensile	20, 200, 400, 600, 700, 850, 1000	n/a	Pipe longitudinal direction
		Isothermal cyclic	20, 200, 400, 600, 700	1.5%	
			20, 400, 600	2.5%	
Weld	Multi-pass	Uniaxial tensile	20 (3 tests)	n/a	Weld longitudinal, extracted from pipe girth weld
	Single-pass	Uniaxial tensile	20, 200, 400, 600, 700, 850, 1000	n/a	Weld longitudinal, extracted from single pass groove weld
			20 (1 test at each condition)	n/a	Weld longitudinal, extracted from single pass groove weld, and “spike-annealed” to 850°C and 950°C respectively
		Isothermal cyclic	20, 200, 400, 600, 700 (3 tests at 20°C)	1.5%	Weld longitudinal, extracted from single pass groove weld

Note: Two tests of each type were performed at each temperature, unless stated otherwise.

Table 2: Fitted Lemaitre-Chaboche model parameters for Esshete 1250 parent material, single C, γ pairs (parent model 1)

T (°C)	σ_o (MPa)	C (MPa)	γ	Q_{inf} (MPa)	b
20	230.0	18,258	92	75.4	21.99
200	151.3	17,896	92	84.6	18.01
400	137.9	15,836	92	120.2	12.56
600	141.4	12,726	92	140.4	16.7
700	148.1	8,712	92	55.0	26.44
850	135.1	2,000	92	0	6.9
1000	47.2	0	92	0	6.9
1100	36.1	0	92	0	6.9
1200	24.9	0	92	0	6.9
1400	2.7	0	92	0	6.9

Table 3: Fitted Lemaitre-Chaboche model parameters for Esshete 1250 parent material, fitted to the monotonic response, two back stresses (parent models 2 and 3)

T (°C)	σ_o (MPa)	C_1 (MPa)	C_2 (MPa)	γ_1	γ_2	Q_{inf} (MPa)[a]	Q_{inf} (MPa)[b]	b
20	150	388,550	12,620	3,478	115.2	119.4	66.8	12
200	100	252,930	15,066	3,478	115.2	124.2	91.8	12
400	100	220,660	13,550	3,478	115.2	167.9	150.1	12
600	75	226,910	13,454	3,478	115.2	166.9	130.2	15
700	75	274,740	9,987	3,478	115.2	61.4	61.4	35
850	75	184,060	2,446	3,478	115.2	0.0	0.0	1.0
1000	47.2	0	0	3,478	115.2	0.0	0.0	1.0
1100	36.1	0	0	3,478	115.2	0.0	0.0	1.0

1200	24.9	0	0	3,478	115.2	0.0	0.0	1.0
1400	2.7	0	0	3,478	115.2	0.0	0.0	1.0

a) Q_{inf} increased to match 2.5% TSR tests – model 2

b) Q_{inf} fitted to 1.5% TSR tests – model 3

Table 4: Fitted Lemaitre-Chaboche model parameters for Esshete 1250 parent material, fitted to cycle 2, two back stresses (parent models 4 and 5)

T (°C)	σ_o (MPa)	C_1 (MPa)	C_2 (MPa)	γ_1	γ_2	Q_{inf} (MPa)[a]	Q_{inf} (MPa)[b]	b
20	110	444,370	62,439	6280.3	388.9	119.8	64.6	24
200	80	290,190	57,990	6280.3	388.9	110.6	78.2	20
400	77	203,090	49,914	6280.3	388.9	180	153.1	7
600	63	344,550	40,841	6280.3	388.9	169.7	125.9	15
700	50	624,610	27,648	6280.3	388.9	48.2	48.2	35
850	50	457,910	7,986.4	6280.3	388.9	0	0	1
1000	47.2	0	0	6280.3	388.9	0	0	1
1100	36.1	0	0	6280.3	388.9	0	0	1
1200	24.9	0	0	6280.3	388.9	0	0	1
1400	2.7	0	0	6280.3	388.9	0	0	1

a) Q_{inf} increased to match 2.5% TSR tests – model 4

b) Q_{inf} fitted to 1.5% TSR tests – model 5

Table 5: Lemaitre-Chaboche parameter fits to Esshete 1250 weld metal behaviour

Model ID	Description
Weld model 1	Historical model, fitted to single-pass MMA weld metal data using a single back-stress, and with Q_{inf} increased to saturate at the 0.2% proof stress of multi-pass weld metal
Weld model 2	*Kinematic parameters fitted to monotonic loading with two back-stresses, with Q_{inf} increased to saturate at the 0.2% proof stress of multi-pass weld metal*
Weld model 3	*Kinematic parameters fitted to monotonic loading with two back-stresses, with no increase to Q_{inf}*
Weld model 4	Kinematic parameters fitted to first re-loading from compression, with two back-stresses, with Q_{inf} increased to saturate at the 0.2% proof stress of multi-pass weld metal
Weld model 5	Kinematic parameters fitted to first re-loading from compression, with two back-stresses, with no increase to Q_{inf}
Weld model 6	Kinematic parameters fitted to first re-loading from compression, with two back-stresses, with σ_0 reduced to simulate as-deposited weld metal, and with Q_{inf} increased further to still saturate at the 0.2% proof stress of multi-pass weld metal
Weld model 7	Kinematic parameters fitted to first re-loading from compression, with two back-stresses, with σ_0 reduced to simulate as-deposited weld metal, and with Q_{inf} increased to saturate at the test levels (ie not MP yield strength)
Weld model 8	Kinematic parameters fitted to first re-loading from compression, with two back-stresses, with σ_0 reduced to simulate as-deposited weld metal, with Q_{inf} increased further to saturate at the 0.2% proof stress of multi-pass weld metal, and with reduced **b** at RT and 200^{O}C
Weld model 9	Kinematic parameters fitted to first re-loading from compression, with two back-stresses, with σ_0 reduced to simulate as-deposited weld metal, with Q_{inf} increased further to saturate at the 0.2% proof stress of multi-pass weld metal, and with **b** halved again at RT and 200^{O}C

Table 6 Fitted Lemaitre-Chaboche model parameters for Esshete 1250 single-pass weld metal, single C, γ pairs (weld model 1)

T (°C)	σ_o (MPa)	C (MPa)	γ	Q_{inf} (MPa)	b
20	287.0	22,324	176	137.0	26.3
200	217.0	21,106	176	132.0	22.9
400	190.0	25,769	176	93.0	15.9
600	189.0	18,377	176	119.4	10.5
700	189.0	14,433	176	104.5	13.7
850	159.0	4,000	176	0.0	0.25
1000	115.0	0	176	0.0	0.25
1100	32.5	0	176	0.0	0.25
1200	22.8	0	176	0.0	0.25
1400	3.2	0	176	0.0	0.25

Table 7: Fitted Lemaitre-Chaboche model parameters for Esshete 1250 single-pass weld metal, fitted to cycle 2, two back stresses (weld models 4 and 5)

T (°C)	σ_o (MPa)	C_1 (MPa)	C_2 (MPa)	γ_1	γ_2	Q_{inf} (MPa)[a]	Q_{inf} (MPa)[b]	b
20	100	395,050	69,079	4,275.8	336.5	44.3	153.4	25
200	120	212,860	56,311	4,275.8	336.5	51.6	164.4	24
400	75	313,530	48,091	4,275.8	336.5	136.4	159.5	4
600	52	428,100	32,781	4,275.8	336.5	138.3	138.3	5
700	65	455,920	25,465	4,275.8	336.5	90.1	90.1	11
850	75	417,910	427	4,275.8	336.5	0.0	0.0	1
1000	53.8	0	0	4,275.8	336.5	0.0	0.0	1

1100	32.5	0	0	4,275.8	336.5	0.0	0.0	1
1200	22.8	0	0	4,275.8	336.5	0.0	0.0	1
1400	3.2	0	0	4,275.8	336.5	0.0	0.0	1

a) Q_{inf} fitted to 1.5% TSR tests – model 5

b) Q_{inf} increased to harden to multi-pass weld 0.2% proof stress – model 4

Table 8: Fitted Lemaitre-Chaboche model parameters for Esshete 1250 single-pass weld metal, fitted to cycle 2, two back stresses, with reduced initial yield stress (weld models 6 to 9)

T (°C)	σ_o (MPa)	C_1 (MPa)	C_2 (MPa)	γ_1	γ_2	Q_{inf} (MPa)[a]	Q_{inf} (MPa)[b]	b[c]	b[d]	b[e]
20	30.0	395,050	69,079	4,275.8	336.5	223.4	114.3	25	10	5
200	59.7	212,860	56,311	4,275.8	336.5	224.8	111.9	24	10	5
400	23.1	313,530	48,091	4,275.8	336.5	211.3	188.2	4	4	4
600	4.4	428,100	32,781	4,275.8	336.5	185.9	185.9	5	5	5
700	15.0	455,920	25,465	4,275.8	336.5	140.1	140.1	11	11	11
850	25.0	417,910	427	4,275.8	336.5	0.0	0.0	1	1	1
1000	22.5	0	0	4,275.8	336.5	0.0	0.0	1	1	1
1100	20.0	0	0	4,275.8	336.5	0.0	0.0	1	1	1
1200	15.0	0	0	4,275.8	336.5	0.0	0.0	1	1	1
1400	3.2	0	0	4,275.8	336.5	0.0	0.0	1	1	1

a) Q_{inf} increased to harden to multi-pass weld 0.2% proof stress – weld models 6, 8, and 9

b) Q_{inf} increased to harden to test limit – weld model 7

c) Fitted test hardening rate – weld models 6 and 7

d) Reduced hardening rate – weld model 8

e) Low hardening rate – weld model 9

11 Figures

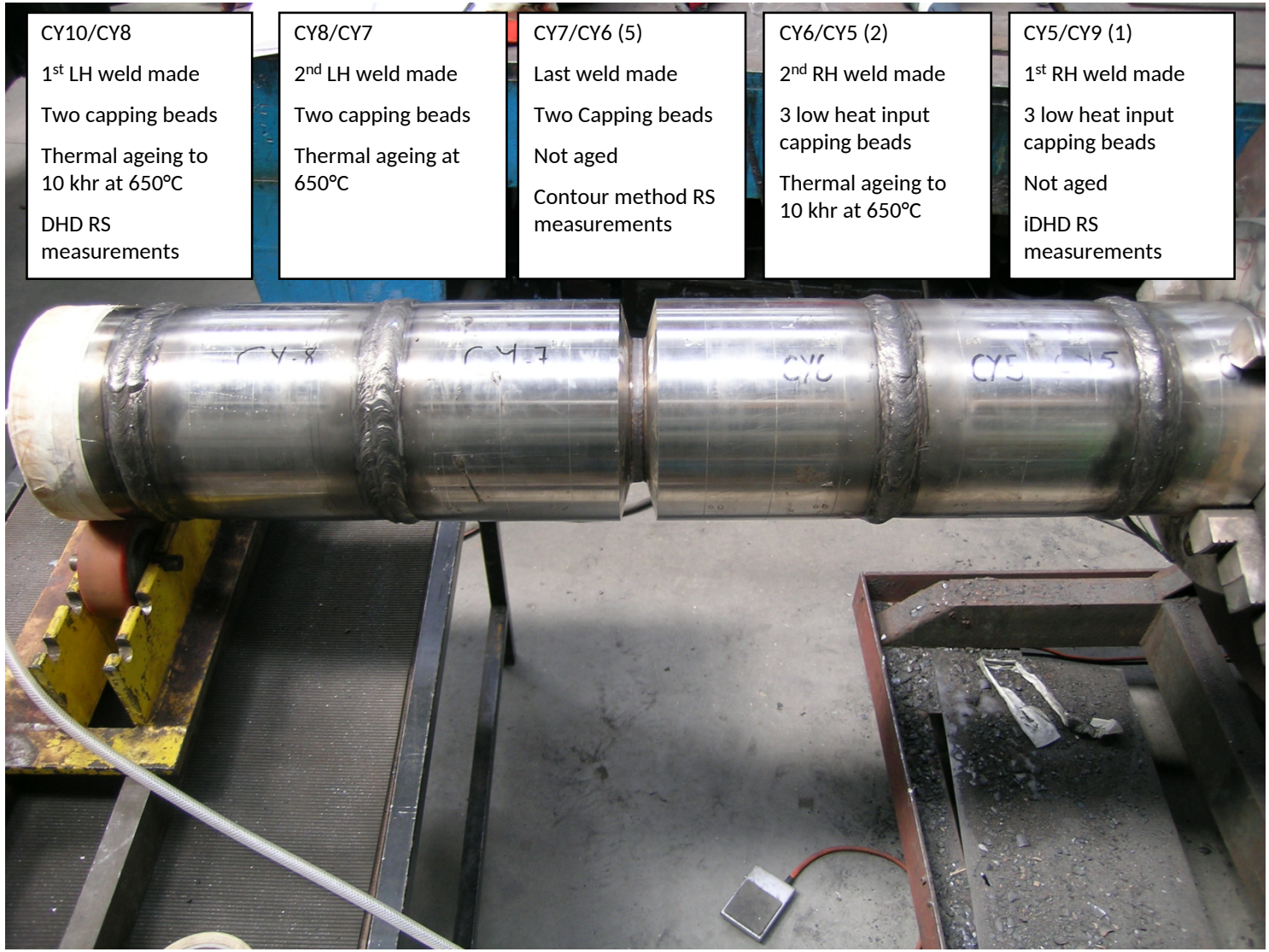

Figure 1: Showing the pipe assembly after completion of the root pass of the last girth weld (CY7/CY6)

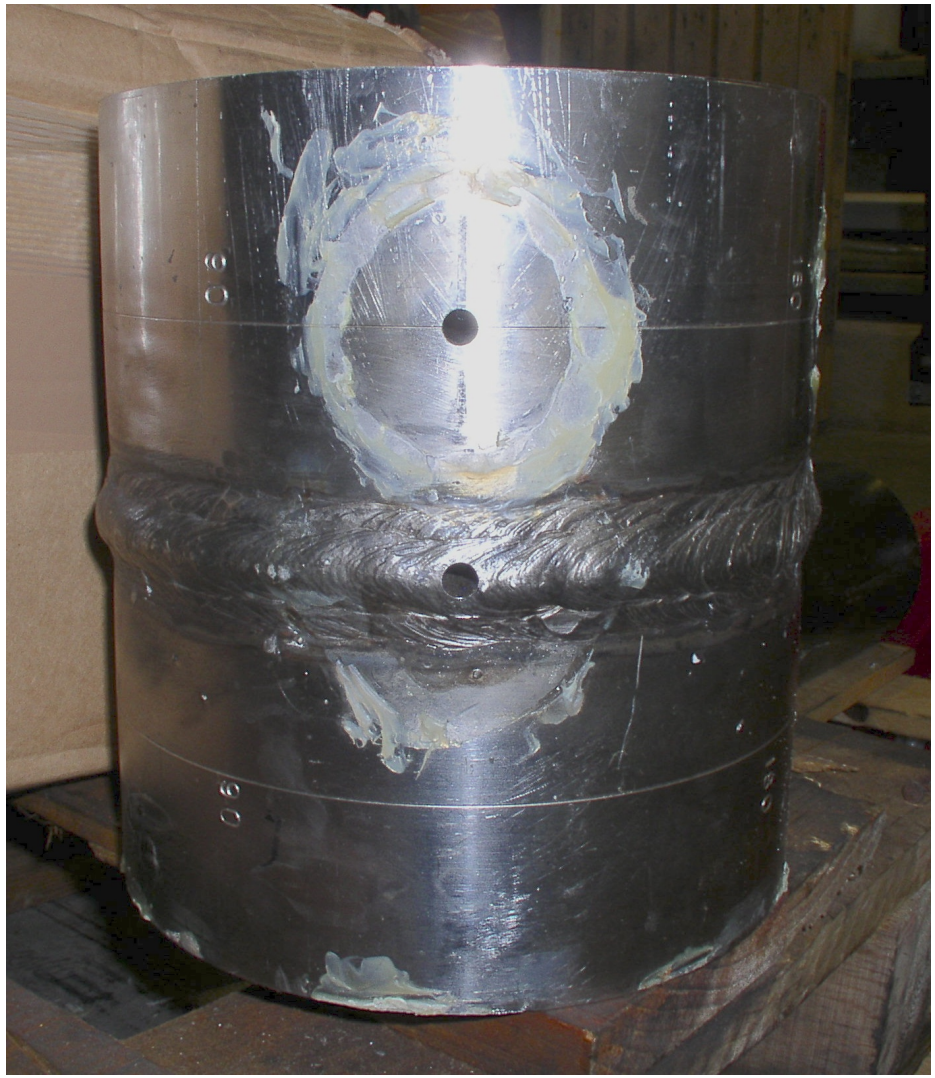

Figure 2: Showing completed short pipe mock-up after iDHD measurements in the as-welded state

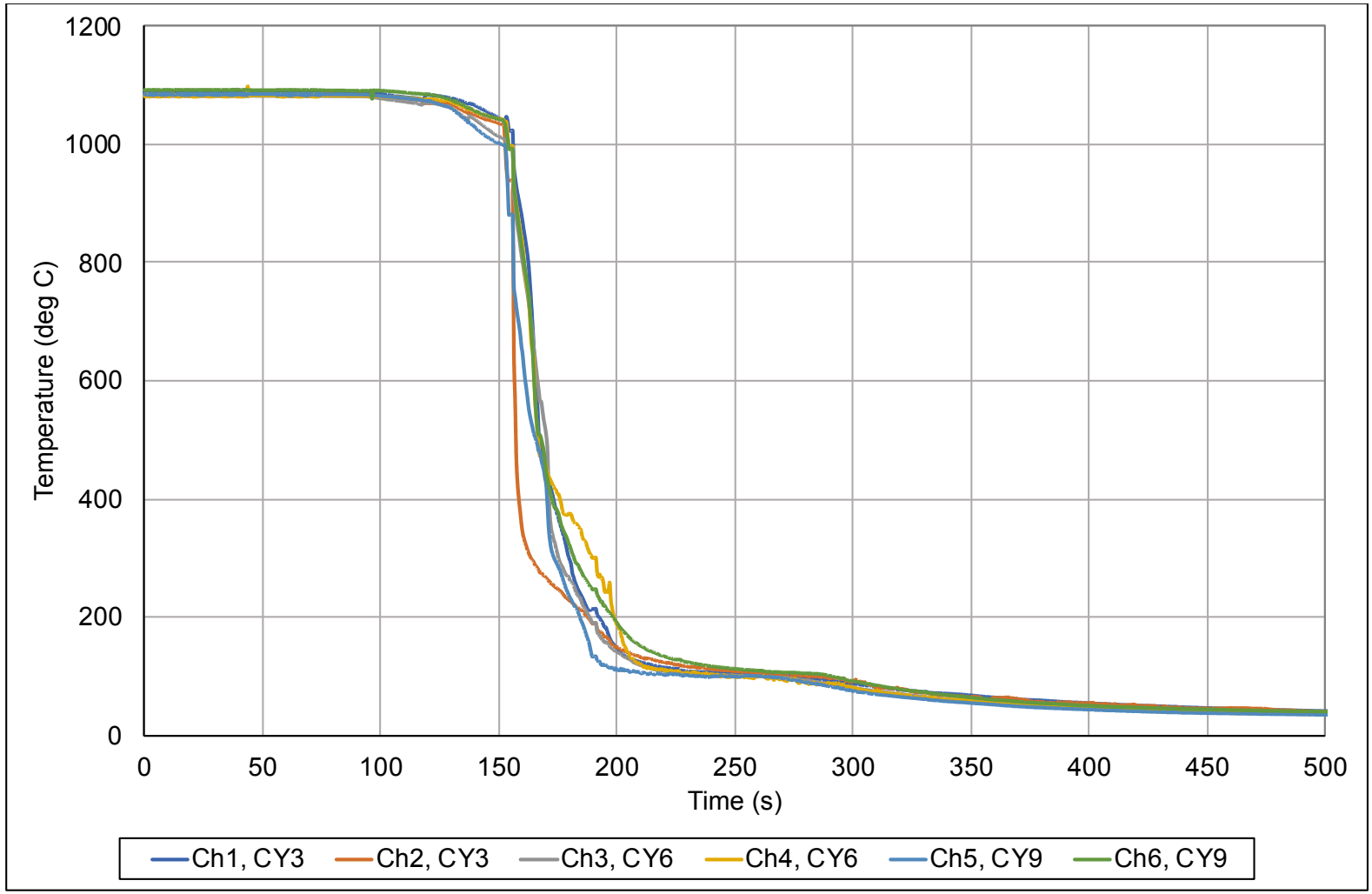

Figure 3: Quench temperature history for short pipe sections

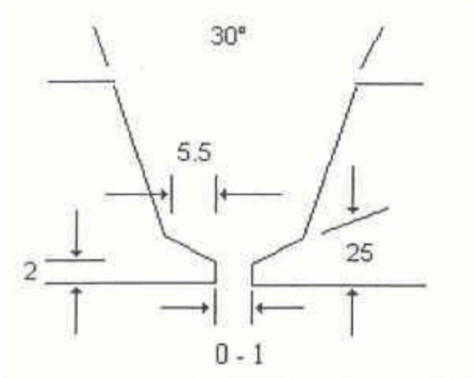

Nominal weld preparation geometry

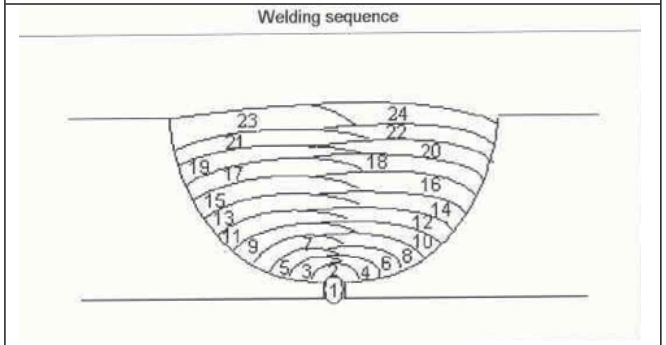

Welding sequence, two capping pass pipe

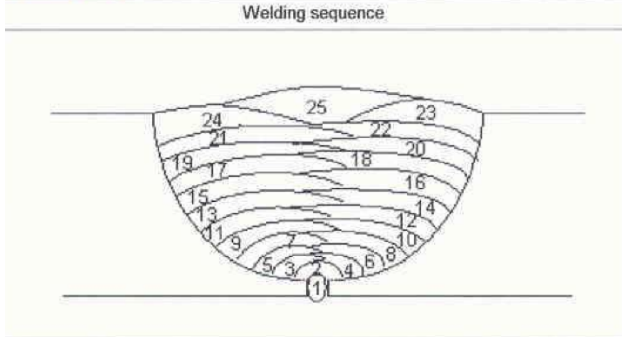

Welding sequence, three capping pass pipe

Transverse micrograph from two-capping pass pipe CY7/CY6

Figure 4: Nominal weld preparation geometry, bead lay-ups and transverse weld macrograph

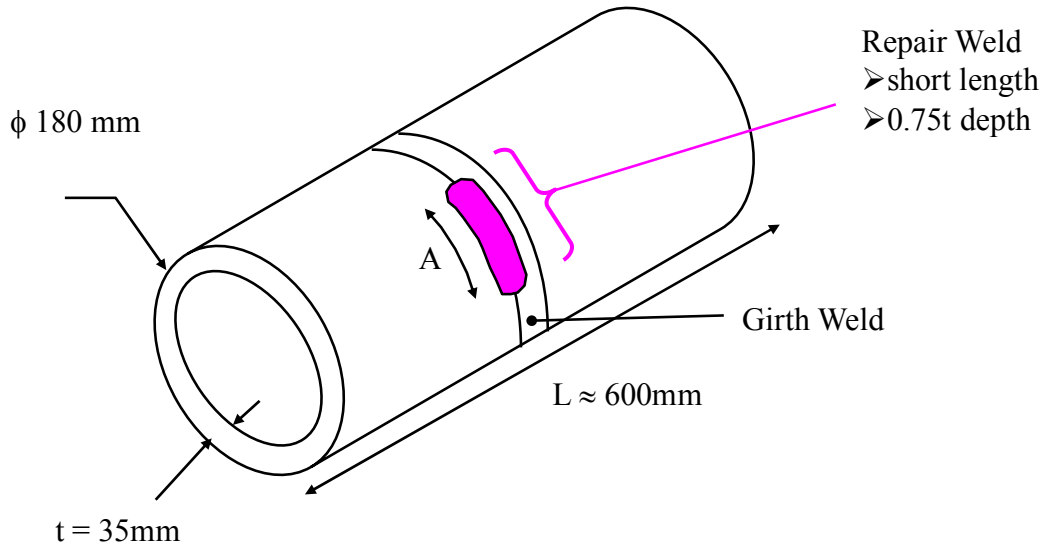

Figure 5: Schematic layout of long pipe mock-up containing a weld repair. The surface length of the repair was approximately 100mm, subtending approximately 60°.

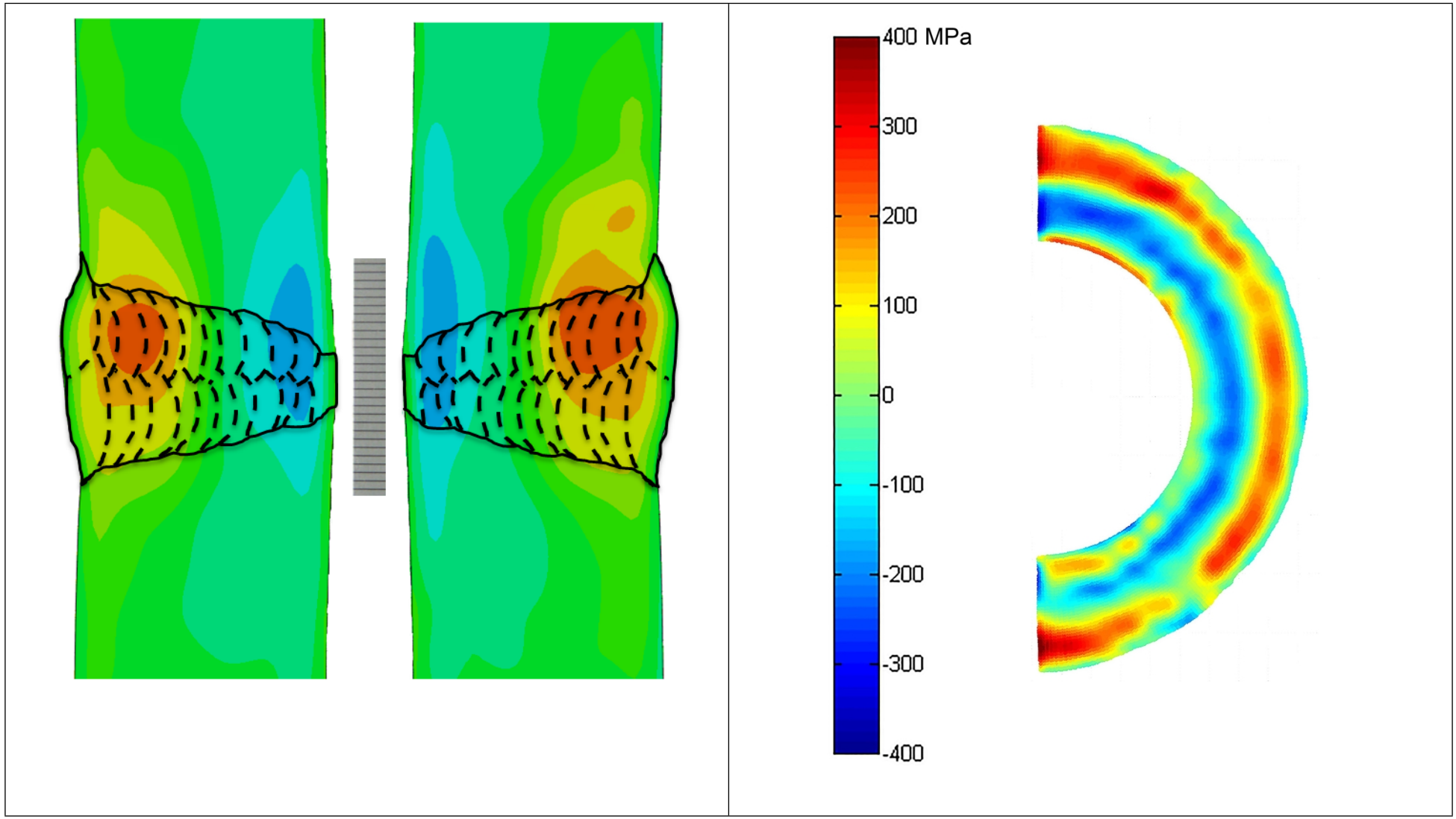

Figure 6: showing hoop (left) and axial (right) stress distributions measured using the contour method on a short Esshete 1250 girth-welded pipe in the as-welded condition

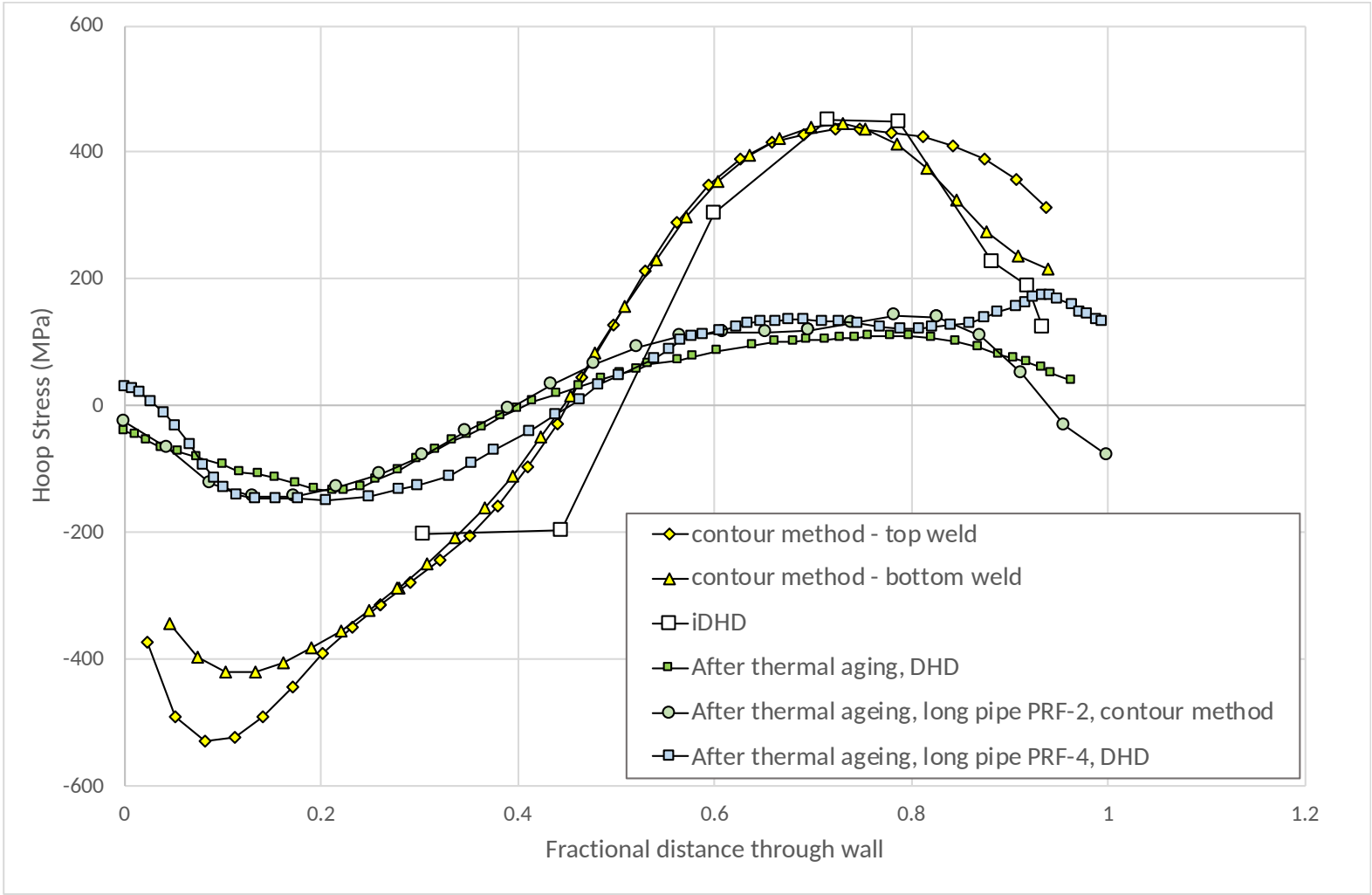

Figure 7: comparing hoop stresses measured in short girth-welded pipes on a through-wall line on the weld centreline in the as-welded condition, using iDHD and the contour method; after thermal ageing at 650℃ for 10 kHr in a short girth welded pipe, using DHD; and after thermal ageing at 650℃ for 20 kHr in the girth welds of long pipes containing weld repairs, using DHD and the contour method.

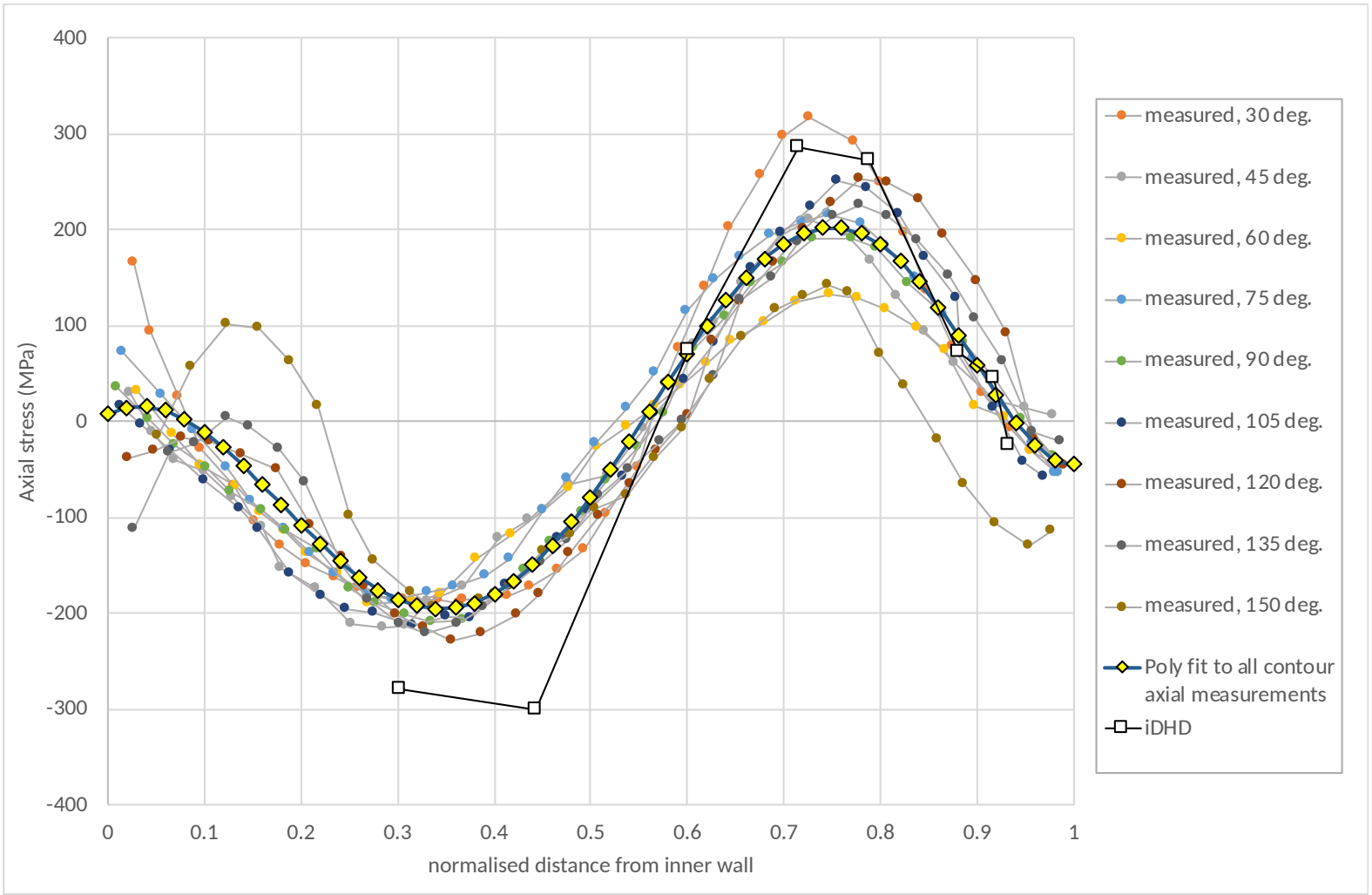

Figure 8: Through-wall distributions of axial stress on the weld centreline of pipe CY7/CY6 in the as-welded condition measured using the contour method at different circumferential locations, compared with both a sixth order polynomial fit to all the individual profiles and an iDHD measurement made on pipe CY5/CY9.

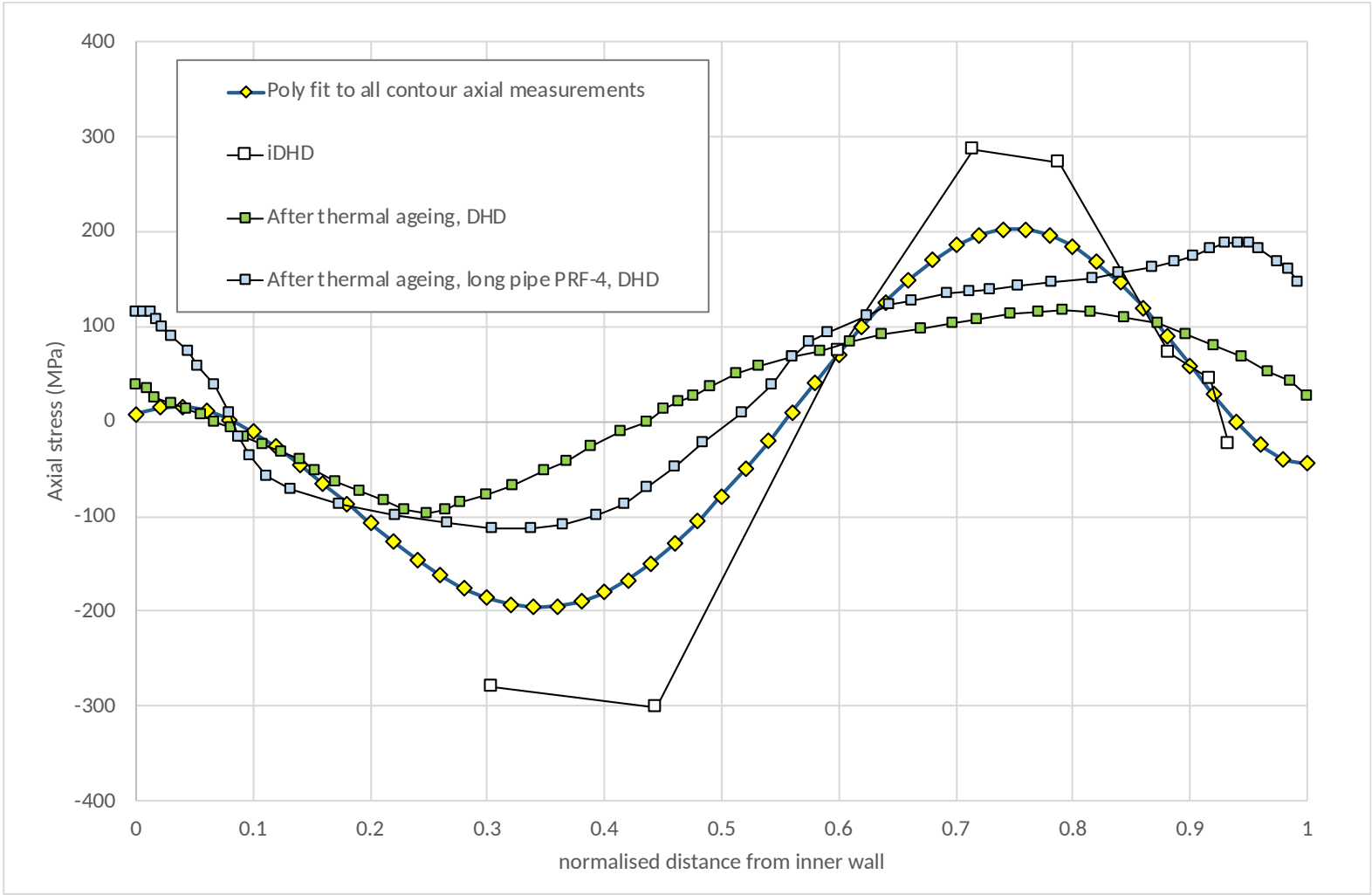

Figure 9: Comparing axial stresses measured in short girth-welded pipes on a through-wall line on the weld centreline in the as-welded condition, using iDHD and the contour method; after thermal ageing at 650℃ for 10 kHr in a short girth welded pipe, using DHD; and after thermal ageing at 650℃ for 20 kHr in the girth weld of af long pipe containing a weld repairs, using DHD.

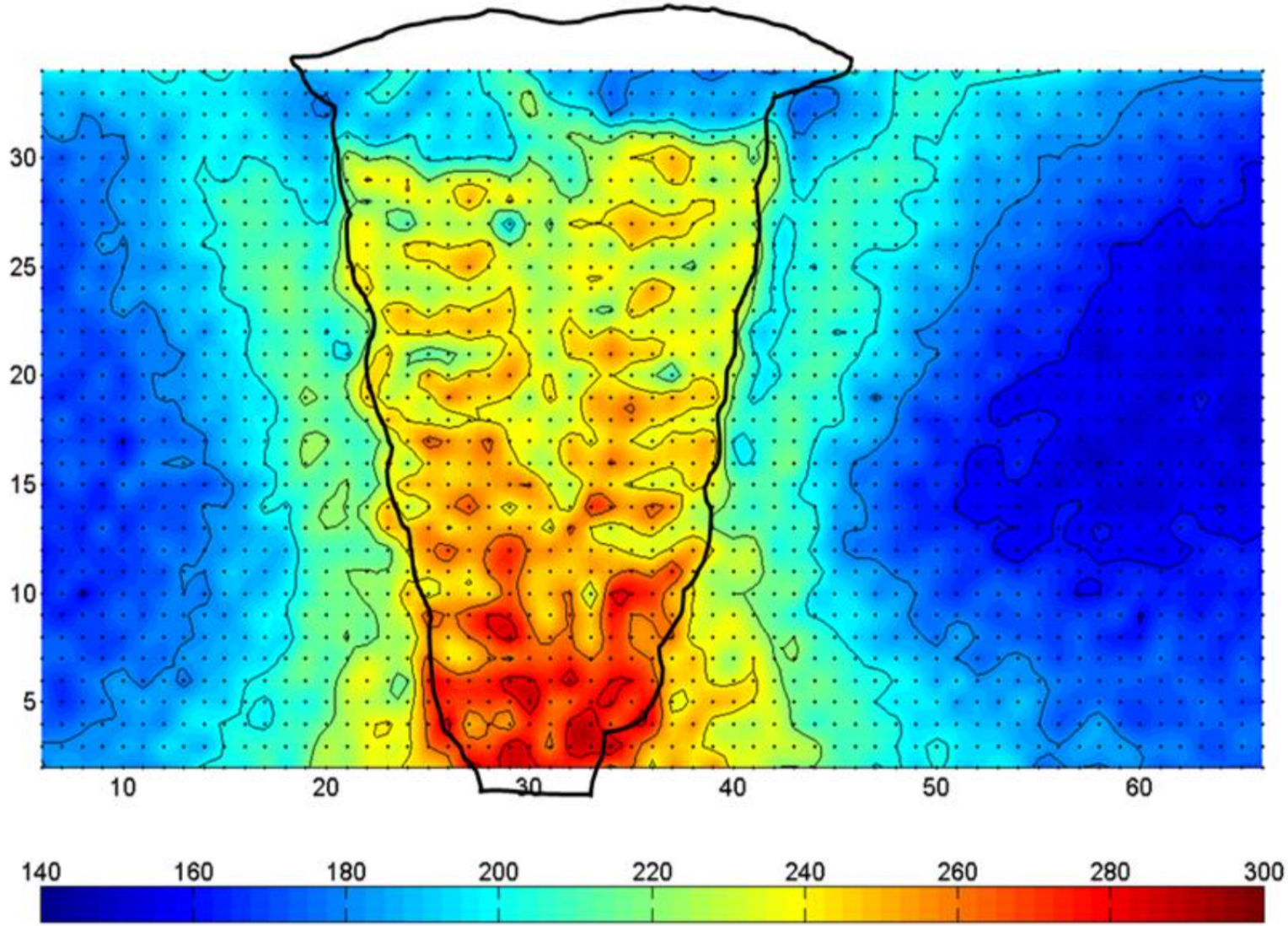

Figure 10: Vickers Hardness map of the weld and HAZ region of Esshete 1250 pipe CY7/CY6 (after[33])

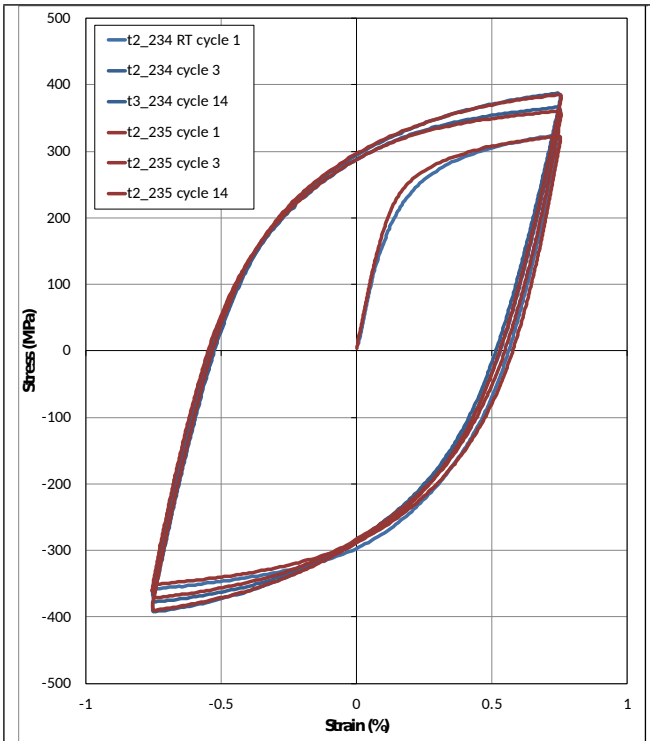

a) Parent material at room temperature, 1.5% TSR

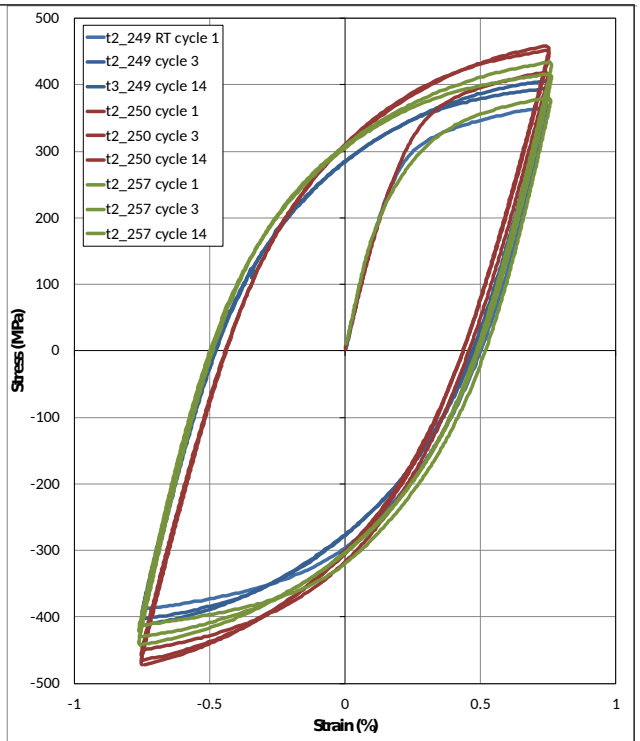

b) Single-pass MMA weld metal at room temperature, 1.5% TSR

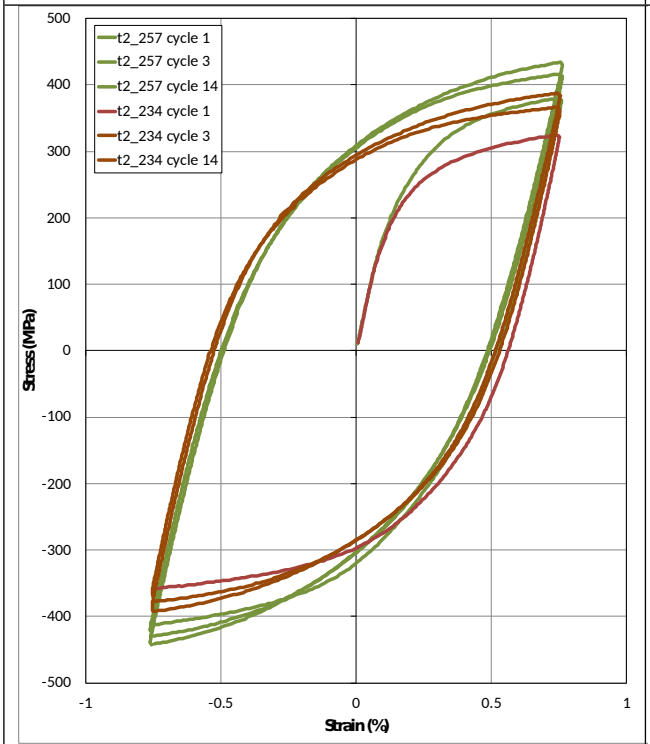

c) Weld (t2_257) and parent (t2_324) at room temperature, 1.5% TSR

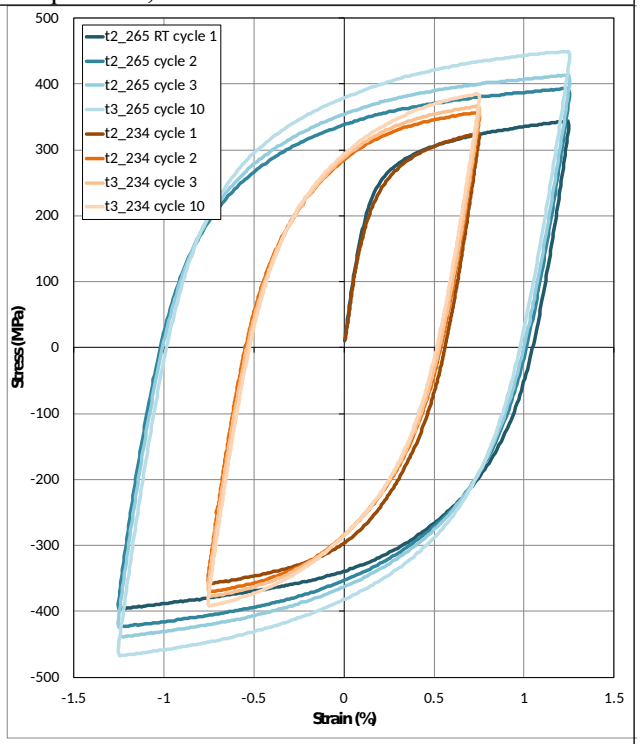

d) Effect of strain range on room temperature parent material response

Figure 11: Isothermal cyclic responses of Esshete 1250 parent and single pass weld metal at room temperature.

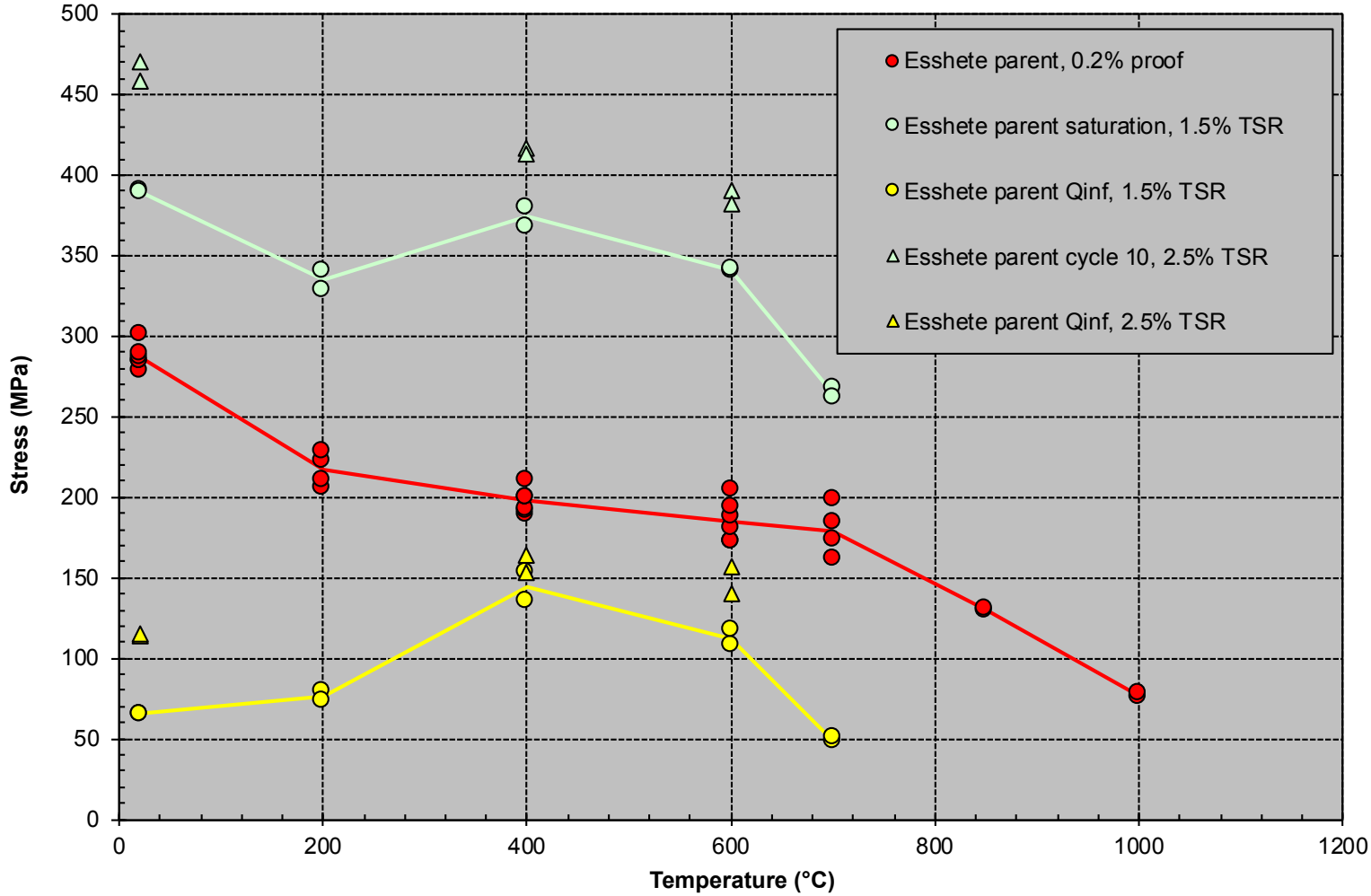

Figure 12: Temperature-dependence of 0.2% proof stress and cyclic hardening saturation limit for Esshete 1250 parent material

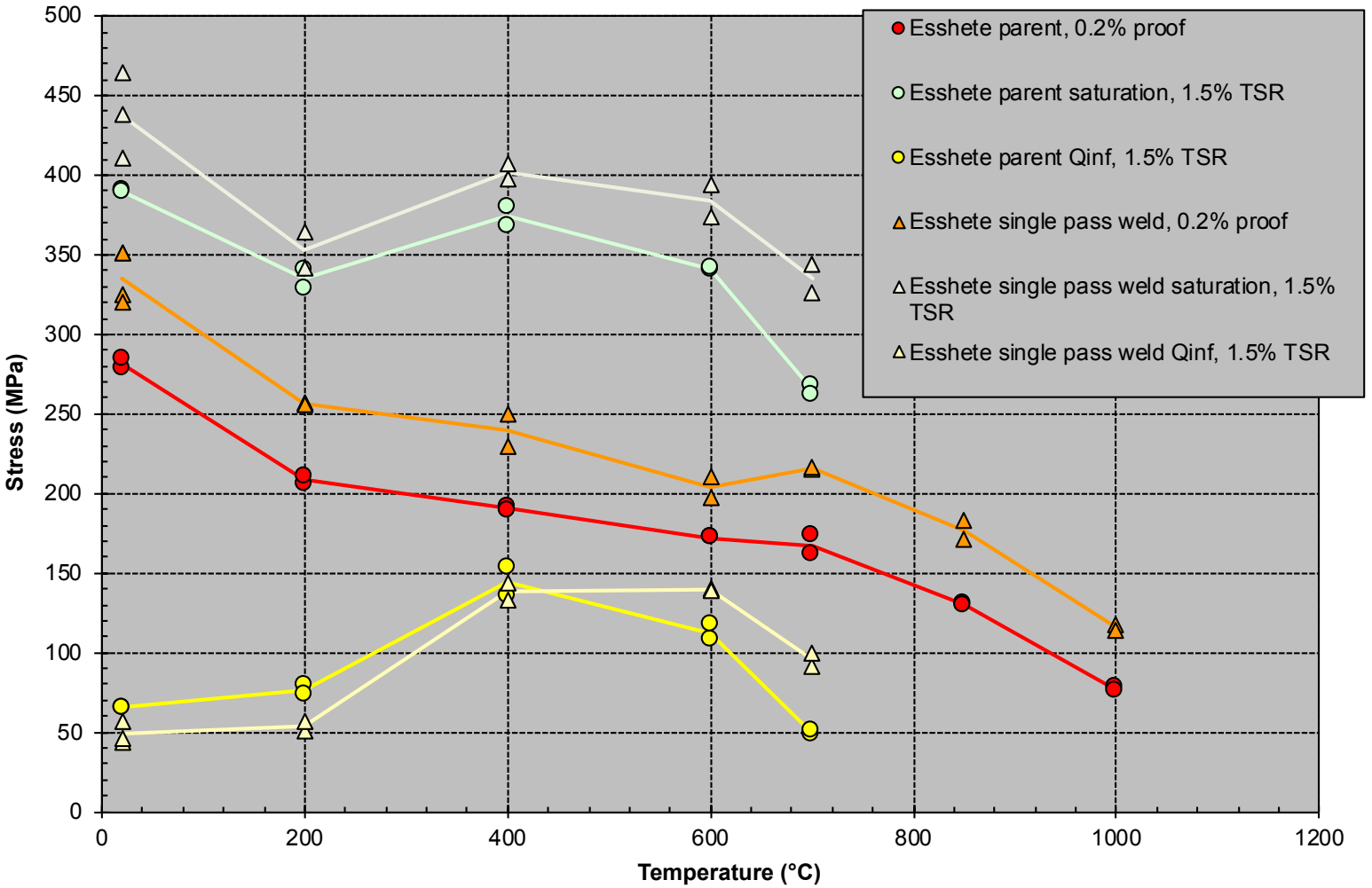

Figure 13: Comparison of the 0.2% proof stress and cyclic hardening saturation limits of Esshete 1250 parent material and single pass MMA weld metal tested under identical conditions

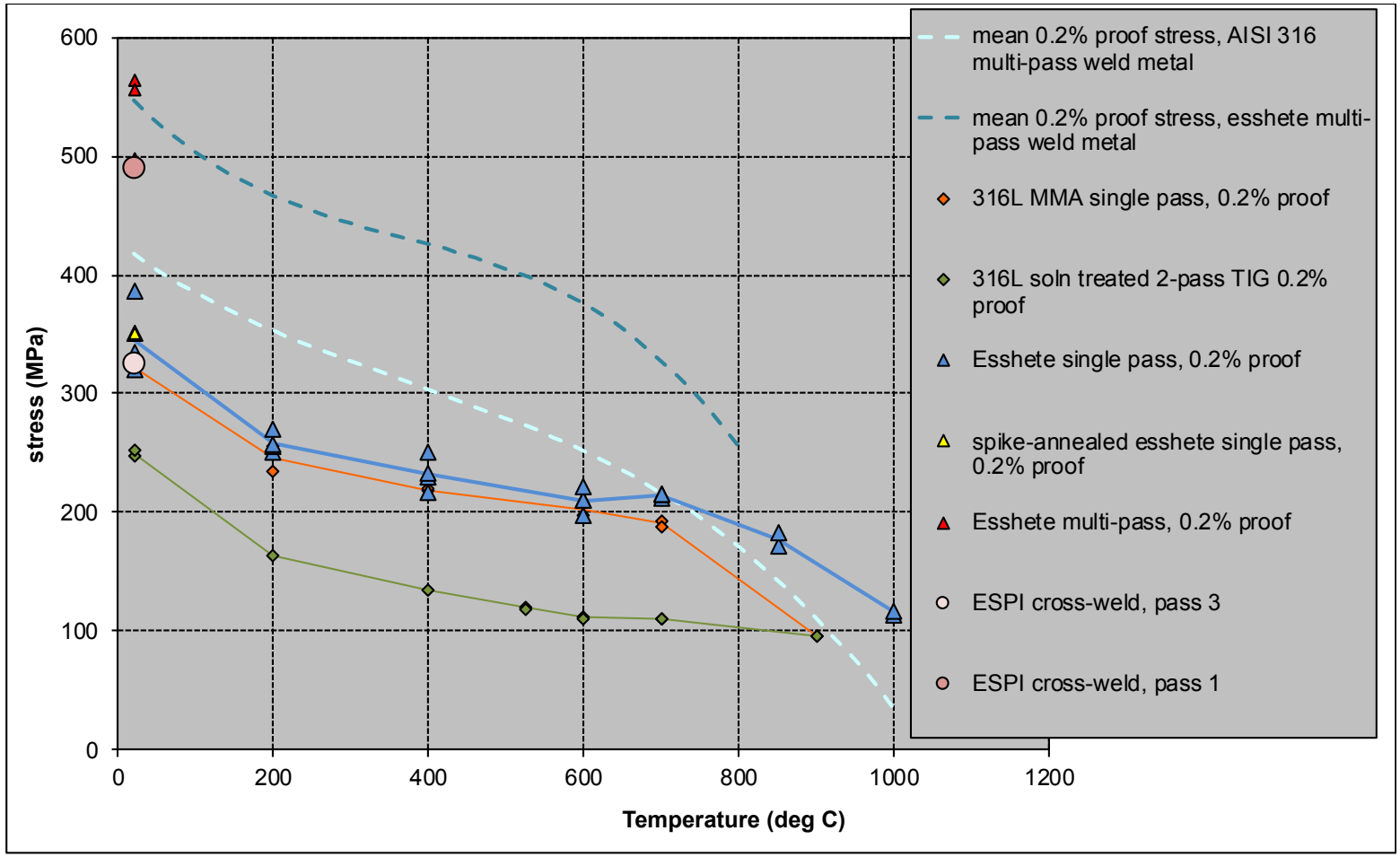

Figure 14: Temperature dependence of 0.2% proof stress for Esshete 1250 and AISI 316L weld metal.

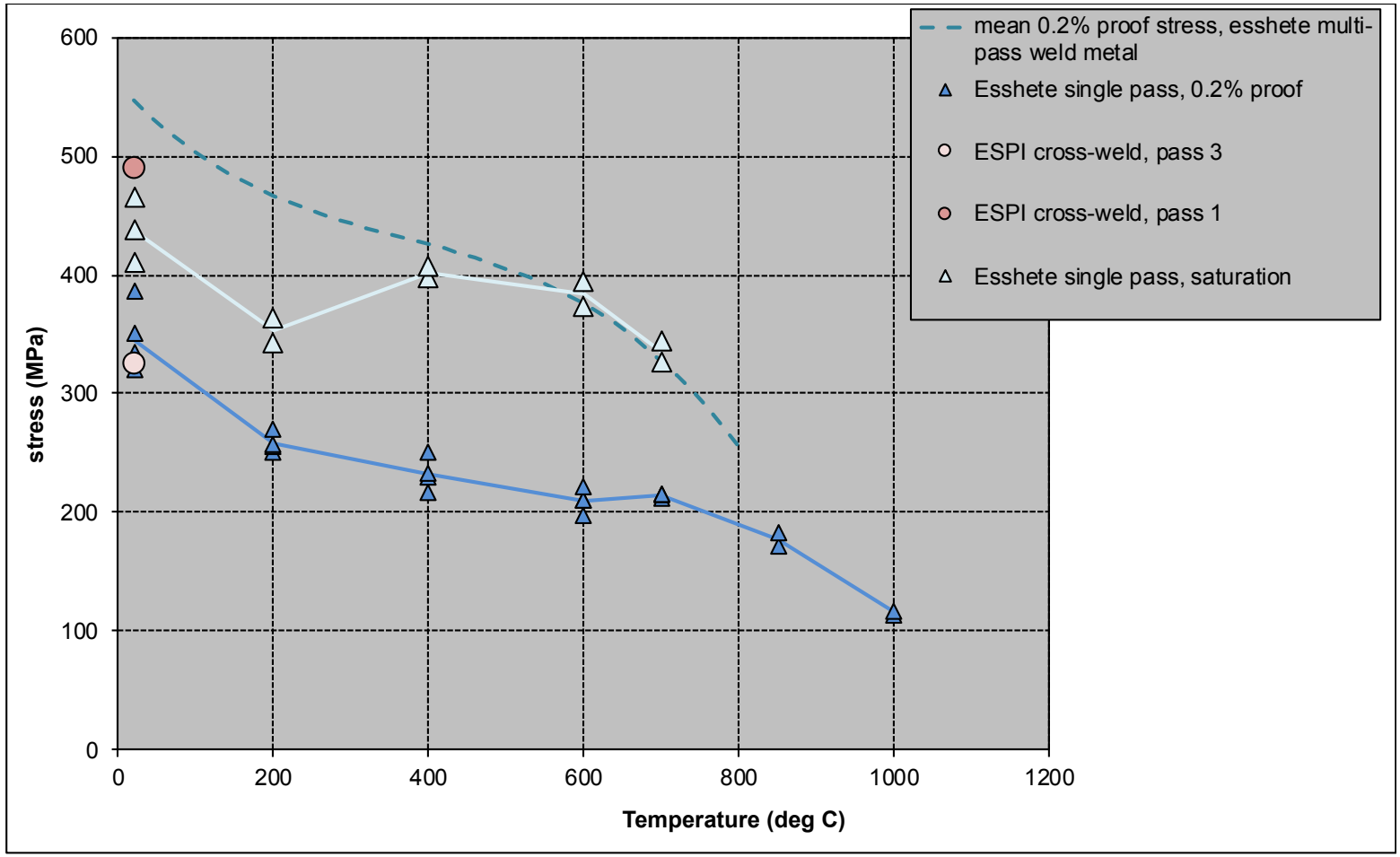

Figure 15: Comparison of the cyclic saturation limit of single-pass Esshete 1250 MMA weld metal with the yield strength of multi-pass Esshete 1250 MMA weld metal

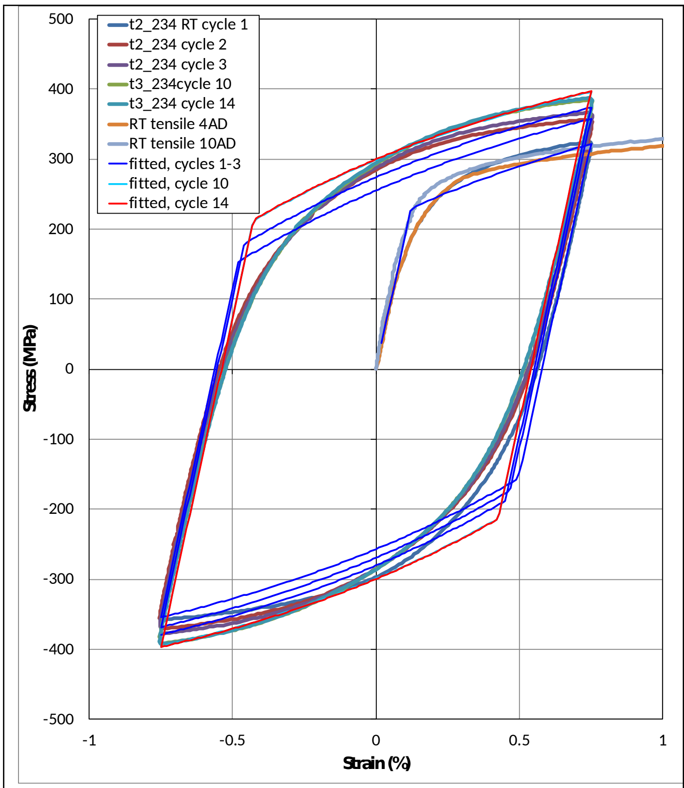

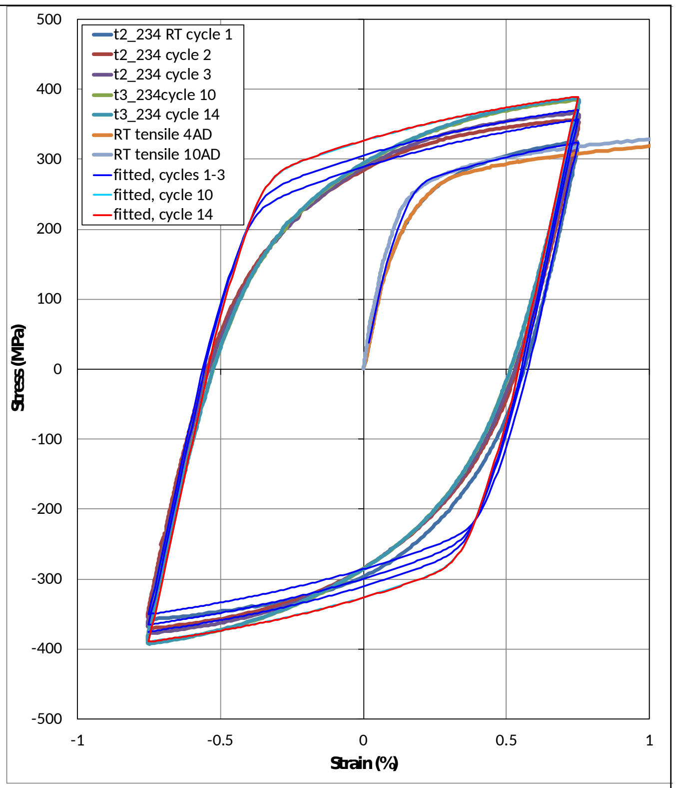

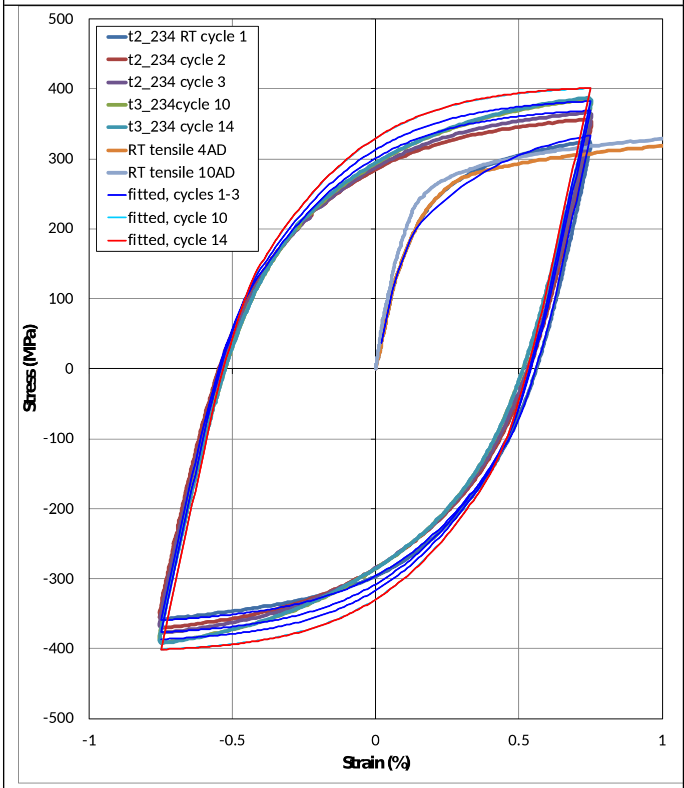

Top Left: “historical” single C-γ fit to monotonic response

Top right: two C-γ pair fit to monotonic response

Bottom left: two C-γ pair fit to first reload into tension(cycle 2)

Figure 16: Showing different Lemaitre-Chaboche parameter fits made to 1.5% TSR cyclic tests on Esshete 1250 parent material at room temperature

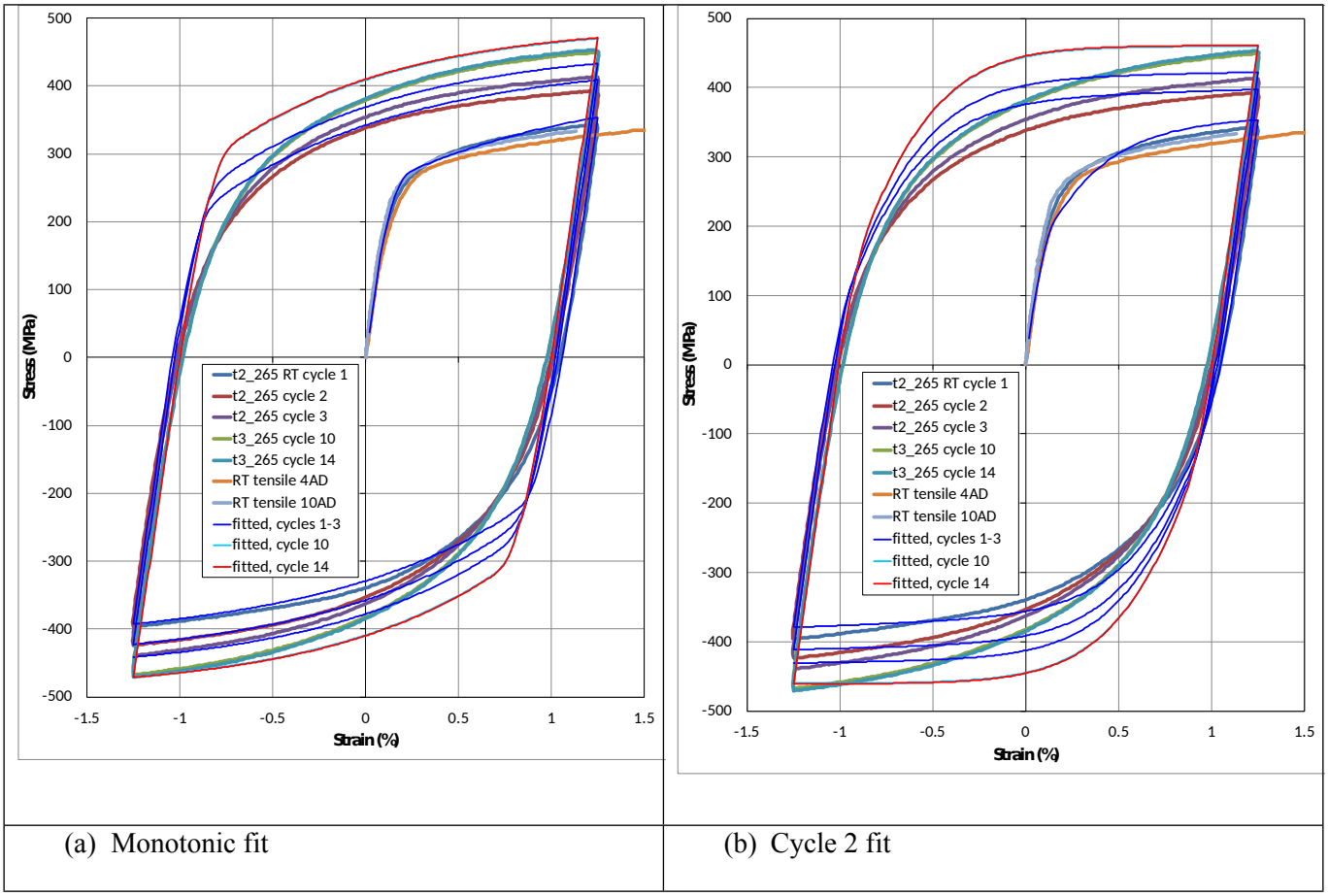

(a) Monotonic fit

(b) Cycle 2 fit

Figure 17: Showing the application of two C-γ pair Lemaitre-Chaboche model fits to predict 2.5% TSR cyclic tests at room temperature in Esshete 1250 parent material

12 Appendix: Welding records

Welding of the pipes was undertaken using MMA and manual TIG techniques. Manual welding is a more variable process than mechanised and automated techniques. Nevertheless, careful records of the welding process were retained, comprising electrode/wie type, average voltage, current and heat input per pass (from which the advance speed could be deduced), interpass temperature, and transverse pass deposition sequence. No records of the bead start/stop positions were kept, meaning that only the capping bead start/stop locations could be identified after welding was complete. The welding records for the two-capping pass weld CY6/7 are given in Table A1 below.

Table A1: weld parameter records for two capping-pass weld

Run	process	wire/elec dia	Layer	V	I	HI	inferred speed
		(mm)		(V)	(A)	(kJ/mm)	(mm/s)
1	TIG	2.4	root	9.7	86	0.98	0.85
2	TIG	2.4	1	10.6	102	0.87	1.25
3	MMA	3.2	2	25.7	121	1.30	2.39
4	MMA	3.2	2	26.9	120	1.48	2.18
5	MMA	3.2	3	26.2	118	1.39	2.22
6	MMA	3.2	3	27.1	119	1.59	2.03
7	MMA	4	4	26	159	1.84	2.25
8	MMA	4	4	26.3	162	1.80	2.37
9	MMA	4	5	26.8	160	1.72	2.49
10	MMA	4	5	26.2	159	1.65	2.52
11	MMA	4	6	26.8	161	1.78	2.42
12	MMA	4	6	26.4	161	1.68	2.53
13	MMA	4	7	26.1	161	1.74	2.42
14	MMA	4	7	25.9	161	1.75	2.38
15	MMA	5	8	26.3	200	2.00	2.63
16	MMA	5	8	26.9	198	1.95	2.73
17	MMA	5	9	26.4	199	1.87	2.81
18	MMA	5	9	26.1	200	1.79	2.92
19	MMA	5	10	26.7	198	1.84	2.87
20	MMA	5	10	25.9	199	1.69	3.05
21	MMA	5	11	26.9	199	1.83	2.93
22	MMA	5	11	25.5	199	1.52	3.34
23	MMA (cap)	5	12	25.9	200	2.46	2.10
24	MMA (cap)	5	12	25.8	201	2.39	2.17